RSC Advances

REVIEW

View Article Online
View Journal | View Issue

Cite this: *RSC Adv.*, 2023, **13**, 33318

Recent advances in biopolymers-based carbon materials for supercapacitors

Hongjie Li, Yanyu Li, Shenmin Zhu,* Yulong Li, Imran Zada* and Yao Li*

Supercapacitors as potential candidates for novel green energy storage devices demonstrate a promising future in promoting sustainable energy supply, but their development is impeded by limited energy density, which can be addressed by developing high-capacitance electrode materials with efforts. Carbon materials derived from biopolymers have received much attention for their abundant reserves and environmentally sustainable nature, rendering them ideal for supercapacitor electrodes. However, the limited capacitance has hindered their widespread application, resulting in the proposal of various strategies to enhance the capacity properties of carbon electrodes. This paper critically reviewed the recent research progress of biopolymers-based carbon electrodes. The advances in biopolymers-based carbon electrodes for supercapacitors are presented, followed by the strategies to improve the capacitance of carbon electrodes which include pore engineering, doping engineering and composite engineering. Furthermore, this review is summarized and the challenges of biopolymer-derived carbon electrodes are discussed. The purpose of this review is to promote the widespread application of biopolymers in the domain of supercapacitors.

Received 11th September 2023
Accepted 27th October 2023

DOI: 10.1039/d3ra06179e

rsc.li/rsc-advances

1. Introduction

Energy plays a pivotal role in contemporary society, but excessive consumption of fossil fuels resulting from rapid global population growth and economic progress in the past few decades has caused a severe ecological crisis.[1] The concern about the deterioration of the natural environment has led mankind to recognize the importance of developing clean energy sources such as hydrogen, wind and solar to replace non-renewable energy sources. Consequently, strategies like sustainable development, carbon neutrality and carbon peaking have been proposed to promote the utilization of clean energy sources.[2,3] However, clean energy production is an intermittent and long-cycle process requiring stable energy storage technology for universal access to clean energy.[4]

Lithium-ion batteries (LIBs) stand as the foremost energy storage devices (ESDs) extensively employed in contemporary applications, whereas their development is constrained by issues such as shortage in lithium metal resources, limitations in overcharging and over-discharging, low output power and challenges in recycling waste batteries.[5] Supercapacitors (SCs) have gained significant interest due to exceptional cycle life,

State Key Laboratory of Metal Matrix Composites, Shanghai Jiao Tong University, Shanghai 200240, China. E-mail: smzhu@sjtu.edu.cn; imranzada99@gmail.com; liyaosjtu@sjtu.edu.cn

Hongjie Li

Mr Hongjie Li received his Bachelor degree in Materials Science and Engineering from Wuhan University of Technology in 2021. He is presently a post-graduate student at the School of Materials Science and Engineering in Shanghai Jiao Tong University. He is currently working on the research of biomass derived porous carbon and their applications in supercapacitors.

Shenmin Zhu

Prof. Shenmin Zhu received her PhD degree from Shanghai Jiao Tong University in 2001. She is presently a professor at the School of Materials Science and Engineering, State Key Lab of Metal Matrix Composites, Shanghai Jiao Tong University. Her current fields of interest are graphene-based functional materials, porous carbon, and bio-inspired photonic crystals with stimuli-responsive properties.

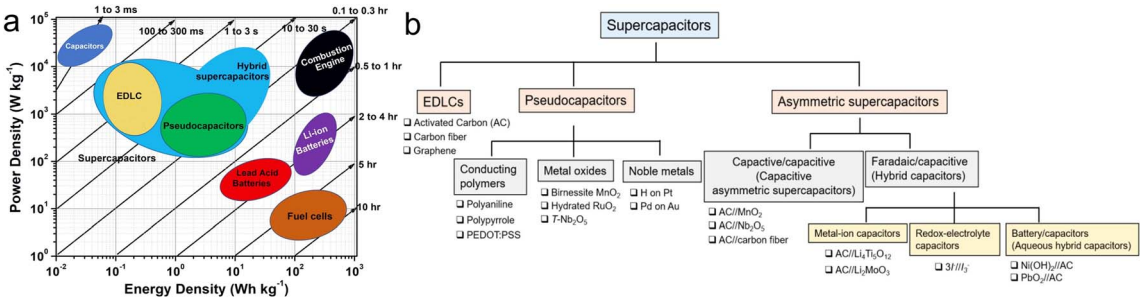

Fig. 1 (a) Ragone diagram of ESDs;[23] (b) classification of SCs and examples of corresponding electrode materials.[5]

excellent power density, affordability and superior safety in comparison to LIBs.[6] Over the past few years, advancements in the sectors of flexible wearable electronic devices, hybrid vehicles and integrated power grids have given rise to novel iterations of SCs, such as metal ion hybrid SCs, micro-SCs and flow SCs.[7] The design of new SCs relies on the innovation of materials. As the core of SCs, electrode materials are crucial for improving electrochemical properties.[8] The main shortcoming of SCs is lower energy density (Fig. 1a),[9] which is affected by the capacitance and voltage window ($E = CV^2/2$).[10] Therefore, there are three strategies to promote the energy density of SCs: (a) preparation of high-capacitance electrode materials, (b) development of electrolytes with wide operating voltage windows and (c) design of new devices.[11,12] This review focuses on biopolymers-based carbon electrodes with high capacitance.

According to the electrode materials employed, SCs can be classified into three main kinds: electric double-layer capacitors (EDLCs), pseudocapacitors (PCs) and asymmetric supercapacitors (ASCs) in Fig. 1b.[5] EDLCs store energy through ion adsorption–desorption at the electrode–electrolyte interface,[13] wherein the electrode predominantly comprises carbon-based materials, encompassing carbon quantum dots, carbon fibers, graphene and activated carbon.[12,14,15] The major advantage of EDLCs is the decent cycle stability, but the poor capacitance leads to the lower energy density of EDLCs (<10 W h kg^{-1}) compared to LIBs (50–1000 W h kg^{-1}).[16] PCs store energy based on rapid and reversible oxidation–redox reactions,[17] and electrode materials for PCs mainly include noble metals (*e.g.*, Pt, Au, *etc.*), transition metal compounds (*e.g.*, Nb_2O_5, RuO_2, $NiCo_2S_4$, Ni_xP_y, *etc.*), alongside conductive polymers such as polyaniline (PANI), polypyrrole (PPy), and polythiophene (PTh).[18–22] The capacitance of pseudocapacitors is generally better than EDLCs, but their limited cycling stability poses challenges for long-term operation. The ASCs consist of two types: capacitor/capacitor and battery/capacitor (hybrid capacitor) whose greatest advantage is to utilize the potential difference between anodes and cathodes to extend the voltage window of ASCs, while taking into account the high capacitance, thus further enhancing the energy density to satisfy the practical requirements.

It is clear from the above that carbon materials are widely applied in SCs. However, traditional carbon electrode materials derived from petroleum-based polymers are difficult to degrade and the resulting waste is a burden to the environment,[24] while the high cost hinders the promotion of SCs, so the identification of cheap and inexpensive carbon precursors is an urgent task. As biologically originated macromolecules, biopolymers have unrivalled advantages owing to their abundant reserves, degradability and renewability. Biopolymers (*e.g.*, cellulose, chitin, lignin, agar, gelatin, keratin, *etc.*) have been reported in works of literature as carbon electrode precursors for SCs.[25] However, the existing articles are more of a review of single biopolymers for SCs and lack overall analysis. Therefore, this

Imran Zada

Dr Imran Zada received his PhD degree in Materials Science and Engineering from Shanghai Jiao Tong University, China, in 2018. Currently, he is working as Postdoctor at the State Key Laboratory of Metal Matrix Composites, Shanghai Jiao Tong University. His research is mainly focused on Bio-inspired materials, Photothermal materials and Energy storage materials for supercapacitors.

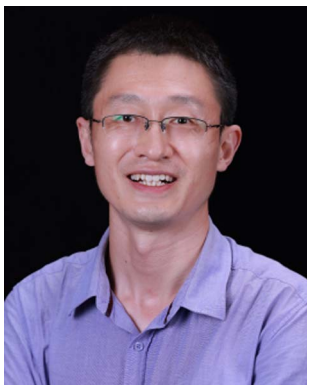

Yao Li

Asso. Prof. Yao Li received his PhD in Material Science from Shanghai Jiao Tong University, China in 2015. He is presently an associate professor at the School of Materials Science and Engineering, State Key Lab of Metal Matrix Composites, Shanghai Jiao Tong University. He is working on the research of bio-inspired material and carbon matrix material, as well as their application in environmental treatment and energy storage.

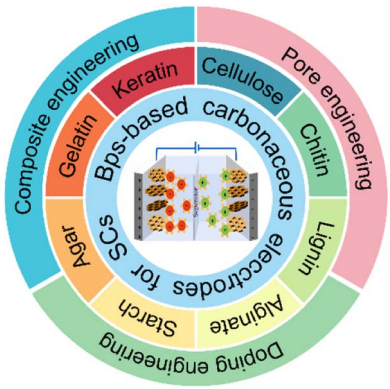

Scheme 1 Illustration of biopolymers-based carbon materials for SCs.

paper reviews research advances in biopolymers-based carbon electrodes for SCs. It is divided into three general parts: (a) review of the recent progress of several types of biopolymers popularly deployed for carbon electrodes in SCs; (b) summary of the approaches to improve the capacitance from three aspects: porous structure design of carbon electrodes, heteroatom doping and multi-component composite;[26] (c) discussion about the challenges and future perspective of biopolymers-based carbon electrode materials Scheme 1.

2. Biopolymers-based electrodes for SCs

Biopolymers have gained significant interest as the precursor of electrode materials for SCs thanks to their advantages of renewable nature, abundant reserves, affordability and non-pollution.[27] In addition, biopolymers can be synthetically transformed into diverse manifestations of carbon-based materials, encompassing carbon microspheres, carbon nanofibers, carbon nanosheets, and carbon aerogels.[28] Meanwhile, biopolymers are rich in heteroatoms, which can contribute to additional pseudocapacitance.[29] Moreover, they carry multiple functional groups (*e.g.*, –OH, –NH_3, –COOH, *etc.*) which can be compounded with other substances through chemical reactions and physical interactions.[30] Considering the diversity of biopolymers, this part mainly focuses on biopolymers derived from biological resources for SCs. Table 1 summarizes the recent progress for biopolymers-based carbonaceous electrode materials for SCs.

2.1 Polysaccharide

2.1.1 Cellulose. Cellulose, primarily derived from the walls of plant cells and microbial tissues, is the most abundant and widely utilized biopolymer, where D-glucose units are connected through β-(1–4) glycosidic bonds.[31] Cellulose is an ideal precursor for carbon electrodes, benefiting from the high carbon content as well as abundant pore structure after a high-temperature reaction.[32] Zhang *et al.* grew glucose-derived porous carbon flakes on cellulose fibers based on the dual effect of $K_3[Fe(C_2O_4)_3]$-catalyzed graphitization and activation, to obtain "mushroom branch"-like porous carbon (CS@CF-KFe, Fig. 2a and b).[33] The CS@CF-KFe exhibited a favorable rate performance (76.8% retention from 1 to 30 A g^{-1}) and outstanding cycle life (100.2% over 10 000 cycles at 100 mV s^{-1}), which are attributed to its lamellar architecture, extended specific surface area (SSA), and abundant micropores facilitating the passage of aqueous ions.

After acid or enzymatic treatment, cellulose has the potential to be transformed into nanocelluloses, which consist of cellulose nanofibers (CNFs), cellulose nanocrystals (CNCs) and bacterial nanocelluloses (BCs).[34] Ding's group developed highly porous carbon (uMPC) with one-step carbonization and activation utilizing compressed BCs as the precursor and thiourea as the doping agent (Fig. 2c).[35] The uMPC possessed ultra-small micropores (−2 nm) and sub-micropores (<1 nm) in Fig. 2d, which improved ion storage and ion/electron diffusion, resulting in the superior capacitance (430 F g^{-1} at 0.5 A g^{-1}) coupled with decent rate capability (76% retention to 10 A g^{-1}) and almost no capacity loss upon undergoing 10 000 cycles.

Moreover, cellulose molecules can be assembled into aerogels with interlinked porous structures because of physical effects, which can effectively accelerate the transport of electrolyte ions, resulting in excellent electrochemical performance.[37] A facile inorganic salt-assisted CNF pyrolysis approach for preparing carbon aerogels (CNFAs) was introduced by Chen's group (Fig. 2e).[36] The large SSA and three-dimensional (3D) porous network provide rich channels of ion transport. The CNFAs realized an improved gravimetric capacitance (440.29 F g^{-1} at 1 A g^{-1}). Furthermore, the corresponding symmetrical supercapacitors (SSCs) delivered a desirable areal energy density (0.081 mW h cm^{-2} at 1.19 mW cm^{-2}), as well as a nearly 100% retention over 7000 cycles.

2.1.2 Chitin and chitosan. Chitin exists in the exoskeletons of arthropods as well as cell walls of fungi, green algae, yeasts and microorganisms, rendering it the second-largest biopolymer after cellulose.[38] Chitin is a decent precursor for nitrogen-doping and its layered structure facilitates the formation of carbon nanosheets for the formation of connected conductive networks, enabling outstanding electrochemical performance.[39] Gao and coworkers synthesized 2D hierarchical porous carbon nanosheets (HPCNs) by hydrothermally treating bulk chitin with phytate assistance followed by carbonization.[40] The HPCNs exhibited ultrathin thickness (3.6 nm), moderate SSA, hierarchical porous architecture and abundant self-doped heteroatoms, resulting in HPCNs-based SSCs achieving a considerable energy density of 23.8 W h kg^{-1} at 215 W kg^{-1}.

Chitosan, the deacetylated derivative of chitin as shown in Fig. 3a, exhibits solubility in acidic solutions to form gels, while it possesses numerous functional groups capable of chelating with metal ions.[41,42] Huang *et al.* reported that chitosan-based hierarchically porous carbon (C-HPC) with exceptional SSA of 3532 m^2 g^{-1} was prepared by dissolving chitosan in acetic acid *via* hydrothermal carbonization and KOH activation (Fig. 3b).[43] The C-HPC demonstrated a superior capacity (455 F g^{-1}), and the assembled SSCs exhibited a maximum energy density of 20.6 W h kg^{-1} at 226.8 W kg^{-1} in 1 M Na_2SO_4. Xi's group employed a facile approach to prepare a composite of CuO/

Table 1 Overview of biopolymers-based carbon electrodes for SCs[a]

Precursors	Electrode materials	SSA ($m^2 g^{-1}$)	C_s ($F g^{-1}$)	E_d ($W h kg^{-1}$)	P_d ($W kg^{-1}$)	Cycle stability	Ref.
Cellulose fibers	CS@CF-KFe	1515.6	313@1 A g^{-1}	21.5	456.6	100.2% (10 000 cycles)	33
BCs	u-MPC	1554	430@0.5 A g^{-1}	0.77 mW h cm^{-2}	17.9 W h L^{-1}	100% (10 000 cycles)	35
BCs	CBC-N@$NiCo_2S_4$	85.2	1078@1 A g^{-1}	42.6	1500	96.8% (5000 cycles)	155
BCs	PANI@CNF/CNS-2	421.4	810@1 A g^{-1}	65.3	800	98% (5000 cycles)	160
CNFs	CNFAs-17%	514.7	440.29@1 A g^{-1}	0.081 mW h cm^{-2}	1.19 mW cm^{-2}	100% (7000 cycles)	36
CNCs	CU-3	366.5	570.6@1 A g-1	—	—	91.2% (1000 cycles)	139
Cellulose	CDC	1381	357@0.5 A g^{-1}	243	492	85% (20 000 cycles)	104
Cellulose	$C_{cel\text{-}LE}$	1893	253@0.1 A g^{-1}	8.77	—	96.5% (10 000 cycles)	110
Cellulose	WC-E-100-48	1418	384 (8.41 F cm^{-2}) @1 mA cm^{-2}	10.97	26.33	86.58% (15 000 cycles)	114
Cellulose	Cell@PPy	139.8	387.6@0.5 A g^{-1}	—	—	92.6% (10 000 cycles)	159
Chitin	HPCNs-800	855	316@5 mV s^{-1}	23.8	215	100% (7000 cycles)	40
Chitin	NSCA-1000	2540	249.4@1 A g^{-1}	26.15	950	98.44% (15 000 cycles)	105
Chitin	HPC-700	1488.3	412.5@0.5A g^{-1}	9.67	—	99.6% (10 000 cycles)	111
Chitosan	C-HPC	3532	455@0.5 A g^{-1}	20.6	226.8	99% (7000 cycles)	43
Chitosan	CuO/Cu@C-700	313.2	2479@0.5 A g^{-1}	76.87	374.5	82.43% (10 000 cycles)	44
Chitosan, SLS	CHPC-800	2700.65	332@1 A g^{-1}	17.7	166.4	97% (10 000 cycles)	46
Chitosan, gelatin	CHPC-0.5	927.17	331@1 A g^{-1}	34	900	97% (10 000 cycles)	47
Chitosan	HPC-1	2787.47	253@0.5A g^{-1}	5.83	4997.1	94.3% (3000 cycles)	99
Chitosan	PBE	1011	250.5@0.5 A g^{-1}	28.3	150.2	107% (5000 cycles)	121
Chitosan	NCSIL-900	301	355@0.2 A g^{-1}	5.83	100	91% (10 000 cycles)	127
Chitosan	APC-2	1650	320@1 A^{-1}	15.82	850	97% (10 000 cycles)	146
Chitosan	BNPC-Fe	806.8	393@0.5 A g^{-1}	19.1	400	103% (8000 cycles)	147
Chitosan	N, S-GHPCF	2279.2	405@1 A g^{-1}	18.4	300	98.8% (10 000 cycles)	149
Chitosan	NiCo-LDH/HPCA-30	1480.47	1504@1 A g^{-1}	33.33	800	90.76% (3000 cycles)	154
Enzymatic lignin	LHC-3K	1660	420@0.1 A g^{-1}	46.8	—	99% (10 000 cycles)	52
Lignin	ACS-600	2237.9	254.2@ 0.2 A g^{-1}	22.4	646	80% (10 000 cycles)	53
Lignin fibers	CF-I-2	712	333@1 A g^{-1}	—	—	100% (2000 cycles)	55
Industrial lignin	C-LRGO41	444.29	330@1 A g^{-1}	11.3	254	100% (2000 cycles)	57
Lignin, CA	CFs-5	837	346.6@ 0.1 A g^{-1}	31.5	400	—	102
Lignin	LDMCN-700-2	1012.5	245@0.5 A g^{-1}	—	—	95.7% (5000 cycles)	109
Lignin	CSH-P.S.-PC-800	3439	—	263.9	700	75.2% (10 000 cycles)	113
SLS	HPCSLS-700-1	903	247@0.05 A g^{-1}	8.4 W h L^{-1}	13.9 W L^{-1}	92% (20 000 cycles)	131
SLS	LSC-ZnC_2O_4/PANI	178	643@1 A g^{-1}	36.3	850.2	88% (5000 cycles)	161
Cobalt alginate	N-PCNFs	283	197@1 A g^{-1}	—	—	91.7% (5000 cycles)	60
Potassium alginate	IPC-800	1145.8	279@1 A g^{-1}	16.9	—	96.6% (10 000 cycles)	61
SA	DSPCs-1	872.6	390.5@0.5 A g^{-1}	10.17	150	100% (10 000 cycles)	62
SA	SAM-700-4	2577.62	441.8@0.5A g^{-1}	20.87	4000	75.11% (5000 cycles)	140
SA	NSC	387	309@0.5 A g^{-1}	15.9 W h L^{-1}	426 W L^{-1}	90% (3000 cycles)	145
SA	$CeCoS_x$-SA/GF aerogels	10.35	873.3@1 A g^{-1}	29.58	801	87.1% (5000 cycles)	59
CA	MXene/CA film	27.3	1244.6 F cm^{-3} @1 A g^{-1}	27.2 W h L^{-1}	—	93.5% (30 000 cycles)	150
Tapioca starch	HPCMS-31	1668	286@0.5 A g^{-1}	8.64	24.7	98% (20 000 cycles)	64
α-starch	SAC-700-50	1863	335.6@0.5 A g^{-1}	7.4	5679.6	96% (20 000 cycles)	65
Starch	I-PCs-0.14	2989	1216@2 A g^{-1}	65.4	787.3	110.2% (10 000 cycles)	66
Starch	st06-900C-HCl	2300	229@ 1 A g^{-1}	—	—	94% (10 000 cycles)	119
β-CD	PMnCD(β)	499	228@1 mA cm^{-2}	25.3	400	>94% (10 000 cycles)	67
β-CD	CDC-MB	1580	291.5@0.5 A g^{-1}	19.7	—	96.3% (10 000 cycles)	68
β-CD	PCD-PC	3710	416@0.5A g^{-1}	23.4	224.9	100% (10 000 cycles)	69
γ-CD	HPC-NS	777	405@1 A g^{-1}	24.3	151	95% (10 000 cycles)	126
Agar	NKAC	2185.5	366.9@0.5A g^{-1}	5.9	103.2	96.4% (10 000 cycles)	71
Agar	BN-PCS	2827.7	361.1@0.5 A g^{-1}	43.5	375	91.1% (10 000 cycles)	72
Collagen	CSGC-700	2419.2	138.8 mA h g^{-1} @ 0.1 A g^{-1}	111.1	165 000	87.2% (10 000 cycles)	75
Collagen	C-G-collagen	1087	365@1 mV s^{-1}	50.69	21.59	97% (10 000 cycles)	76
Gelatin	HPC-3.5	2473	216.5 @1 A g^{-1}	108.6	961.1	84.4% (10 000 cycles)	79
Gelatin	1G-30SC-750	350	215@0.1 A g^{-1}	—	—	97.4% (10 000 cycles)	81
Gelatin	Ni_2P-CNFs-700	12.9	145 mA h^{-1} @0.5 A g^{-1}	42	413	88% (6000 cycles)	156
Fibroin	NPC-750	80.4	565.3@1 A g^{-1}	26.2	263.9	93.3% (10 000 cycles)	83

Table 1 (*Contd.*)

Precursors	Electrode materials	SSA (m^2 g^{-1})	C_s (F g^{-1})	E_d (W h kg^{-1})	P_d (W kg^{-1})	Cycle stability	Ref.
Fibroin, CNFs	NPCN-50	1882	329.9@0.25 A g^{-1}	37.5	186.3	99.5% (5000 cycles)	84
Keratin	H_2SO_4-KK-3	2864	270@1 A g^{-1}	11.84	8525	98% (10 000 cycles)	87
Keratin	HHC9K4	1548	999@1 A g^{-1}	32	325	98% (10 000 cycles)	88

[a] Note: SSA: specific surface area; C_s: specific capacitance; E_d: energy density; P_d: power density; CNFs: cellulose nanofibers; BCs: bacterial nanocelluloses; CNCs: cellulose nanocrystals; SLS: sodium lignosulfonate; CA: cellulose acetate; SA: sodium alginate; CD: cyclodextrin.

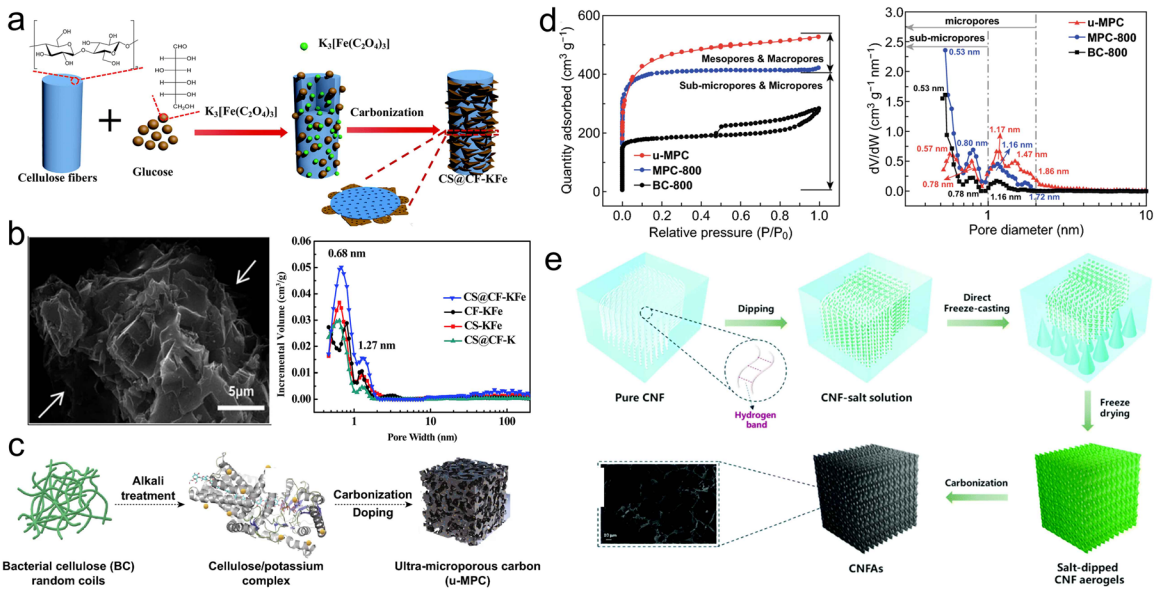

Fig. 2 (a) Synthetic route for the synthesis of CS@CF-KFe; (b) SEM and pore size distribution (PSD) plots of CS@CF-KFe;[33] (c) schematic for the synthesis of u-MPC; (d) nitrogen adsorption–desorption and PSD curves of samples;[35] (e) preparation process of CNFAs.[36]

Cu@C, achieved through the chelation of Cu^{2+} with chitosan.[44] Chitosan was transformed into the N-doped carbon framework and copper precursors into CuO/Cu nanoflowers. Remarkably, CuO/Cu@C-700 carbonized at 700 °C developed a capacity of 2479 F g^{-1} at 0.5 A g^{-1}, and corresponding ASCs exhibited an impressive energy density (76.87 W h kg^{-1} at 374.5 W kg^{-1}) on account of 3D interconnected porous structure and favorable SSA.

Moreover, chitosan is a polycationic polymer that can self-assemble with polyanionic polymers under acidic conditions,

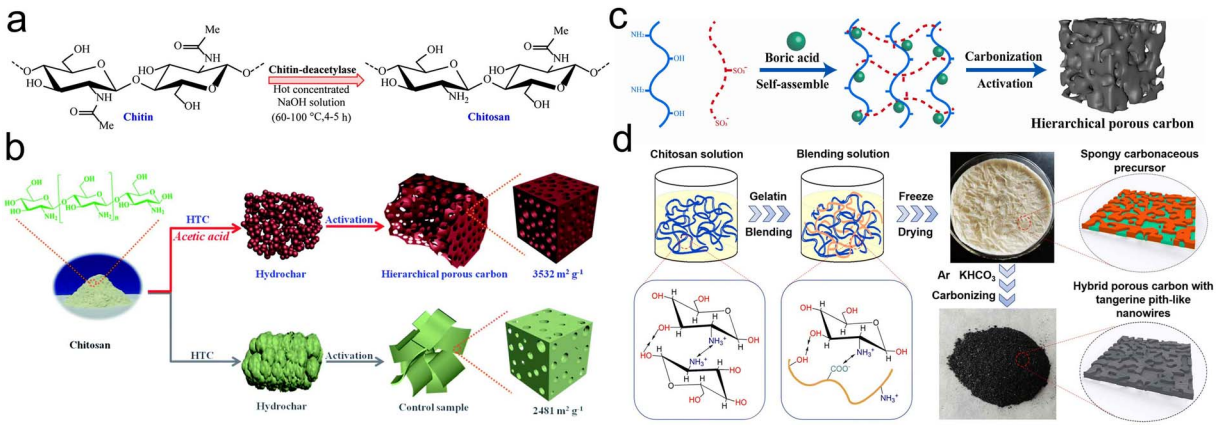

Fig. 3 (a) Process of deacetylation of chitin for the fabrication of chitosan;[42] (b) diagram for the construction of CHPC;[43] (c) preparation mechanism diagram of CHPC-800;[46] (d) scheme for the synthesis procedure of CHPC-0.5.[48]

leading to form co-doped porous carbon.[45] Sun and coworkers constructed the 3D porous carbon (CHPC) doped N, B and S by self-assembling sodium lignosulfonate (SLS) with chitosan at the aid of boric acid (Fig. 3c).[46] The CHPC-800 activated at 800 °C a suitable capacity of 332 F g^{-1} at 1 A g^{-1}, still remaining 267 F g^{-1} at 20 A g^{-1}. Yuan *et al.* synthesized hierarchical porous carbon (CHPC) by combining chitosan with gelatin (Fig. 3d).[47] Benefiting from high heteroatom content, SSA and appropriate average pore size, the optimal sample yielded a remarkable capacitance (331 F g^{-1} at 1 A g^{-1}) with decent rate capability and mechanical stability.

2.1.3 Lignin. Lignin is an abundant class of aromatic polymers whose structure is forged by phenyl-propane structural units, specifically guaiacol (G), syringyl (S) and *p*-phenyl hydroxyl (H) *via* carbon–carbon and ether bonds (Fig. 4a).[49] Lignin interacts with cellulose and hemicellulose to ensure the toughness of cell wall.[50]

Lignin is ideal for preparing carbon electrodes with large carbon yields and active functional groups.[51] Guo and coworkers transformed enzymatic lignin into 3D porous carbon (LHC) possessing a generous SSA (1660 m^2 g^{-1}) by hydrothermal carbonization and KOH activation (Fig. 4b), realizing a desirable capacity of 420 F g^{-1}. The corresponding SSCs delivered an energy density of 46.8 W h kg^{-1} in ionic liquid.[52] Wang *et al.* obtained monodisperse lignin-derived blueberry-like porous carbon nanospheres (ACS) through a four-step process as shown in Fig. 4c.[53] The ACS-600 carbonized at 600 °C achieved an impressive capacitance (254.2 F g^{-1} at 0.2 A g^{-1}) in 6 M KOH. The SSCs assembled with ACS-600 delivered a voltage range from 0 to 2 V and energy density was up to 22.4 W h kg^{-1} in 1 M Na_2SO_4. However, the amorphous structure of lignin after carbonization seriously hinders the migration and diffusion of electrolyte ions, so it is necessary to modify lignin.[54] Han *et al.* demonstrated a simple method of iodinating lignin fibers (Fig. 4d), where a π–π conjugated structure was formed, enhancing intermolecular interactions and allowing the precursors to maintain original morphology.[55] The carbon fibers maintained exceptional graphitization and proper SSA, leading to an enhancement in capacitance with a value of 333 F g^{-1} at 1 A g^{-1}.

Furthermore, compounding lignin to 2D materials can optimize the structure of lignin while also helping to alleviate the stacking problem of 2D materials.[56] Jiang *et al.* chose industrial lignin as the carbon precursor and reducing agent to achieve an ordered modification of lignin on the rGO surface through hydrothermal reaction followed by carbonization, which not only suppressed the stacking of rGO nanosheets but also avoided self-aggregation of lignin after carbonization.[57] The lignin/rGO generated porous structures during no-activator carbonization, exhibiting an impressive capacitance of 330 F g^{-1} at 1 A g^{-1} and durable cyclability as evidenced by retaining 100% of initial capacity after enduring 10 000 cycles.

2.1.4 Alginate. Alginate, derived from brown algae or Sargassum, is a class of linear anionic biopolymers. The alginate molecular chain is composed of the homopolymerized region (G) of α-L-glucuronic acid residue, the homopolymerization region (M) of β-D-mannuronic acid residue, and the hetero-polymerization region (GM) connected by (1 → 4) glycosidic bond (Fig. 5a).[58,59]

The functional groups in the G region of alginate enable cross-linking with metal ions to realize the "egg-shell" structure, which can be employed to achieve effective loading of metal compounds on carbon substrates, alleviating the problems of low multiplicity and poor electrical conductivity of pseudocapacitive materials. Guo *et al.* put forward a facile *in situ* synthesis strategy to construct N, S doped porous $CeCoS_x$-SA/GF

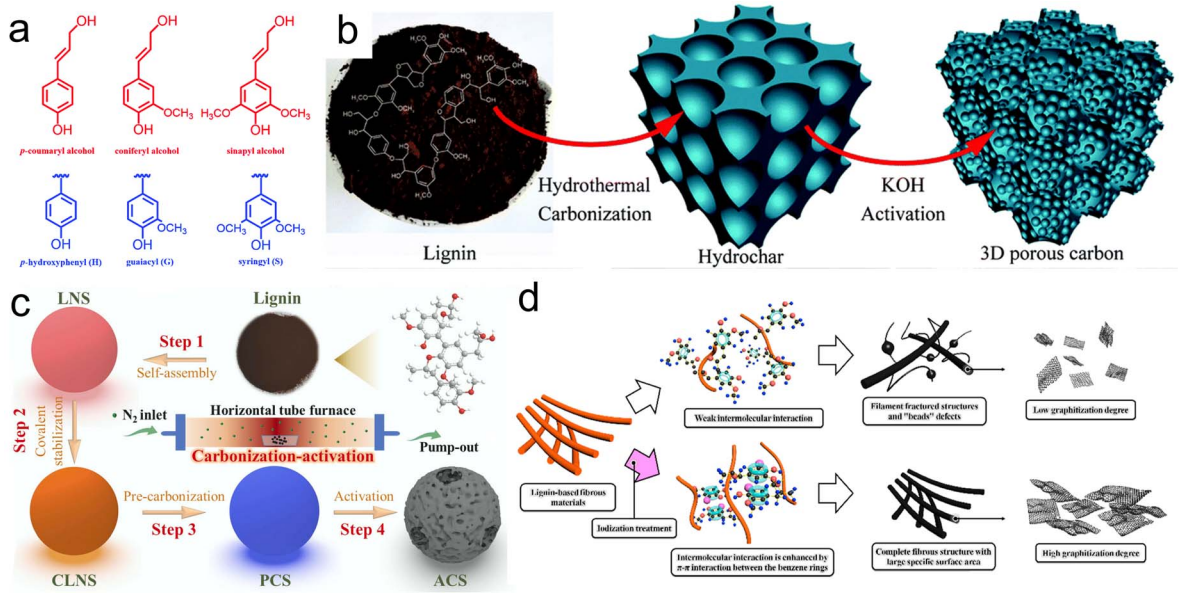

Fig. 4 (a) Monomer units and precursors of lignin;[49] (b) illustration for the fabrication of LHC;[52] (c) diagram for the synthesis of ACS-600;[53] (d) structure comparison between carbon fibers by iodization and original carbon fibers.[55]

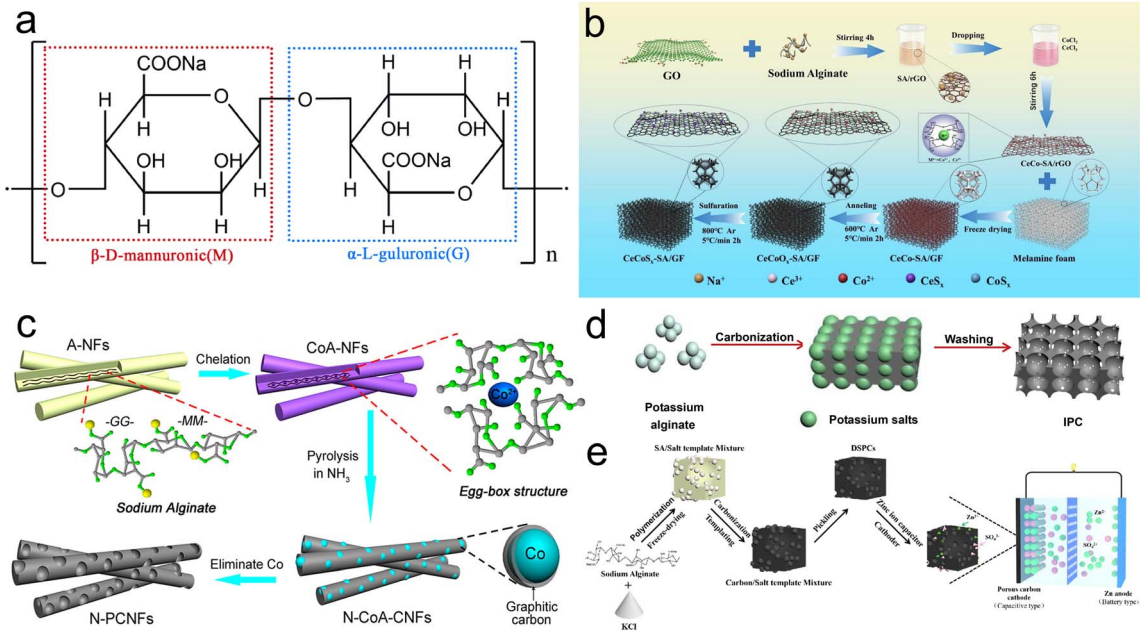

Fig. 5 (a) Chemical formula of alginate; (b) diagram for the stepwise preparation of $CeCoS_x$-SA/GF;[59] (c) illustration for the synthesis of N-PCNFs;[60] (d) schematic for the construction of IPC-800;[61] (e) schematic diagram for the synthesis of DSPCs.[62]

aerogels based on the pairing principle of sodium alginate (SA) with Ce^{3+} and Co^{2+} and the dispersion effect of melamine foam on graphene (Fig. 5b).[59] The $CeCoS_x$-SA/GF exhibited an outstanding capacity (873.3 F g^{-1} at 1 A g^{-1}), complemented by the capacity retention of 87.1% after 5000 cycles, and the ASCs where $CeCoS_x$-SA/GF was applied as the positive electrodes exhibited a remarkable energy density (29.58 W h kg^{-1} at 801 W kg^{-1}). Furthermore, the characteristic for cross-linking alginate with metal ions is also frequently applied to pore engineering. Li's group prepared nitrogen-doped porous graphitic carbon nanofibers (N-PCNFs) with large-size mesopores (10–40 nm) utilizing the cross-linking of SA with Co^{2+} (Fig. 5c).[60] The N-PCNFs realized a moderate capacitance (197 F g^{-1} at 1 A g^{-1}) and retained 91.7% of initial capacity over 5000 cycles in the two-electrode system.

Furthermore, alginate also is the self-template and self-activator for pore engineering. Sun's group prepared 3D interlinked porous carbon (IPC) using one-step carbonization with potassium alginate as the precursor and self-activator (Fig. 5d).[61] The IPC-800 carbonized at 800 °C showed a favorable capacitance (279 F g^{-1} at 1 A g^{-1}), together with exceptional rate performance and outstanding cycling stability. In another work, Hu *et al.* prepared microporous-dominated porous carbons (DSPCs) derived from SA using Na^+ and KCl for etching the carbon skeleton to increase SSA and modulate the structure (Fig. 5e).[62] The corresponding SSCs and aqueous zinc ion capacitors (ZIHCs) assembled with DSPCs gave the energy storage of 10.17 W h kg^{-1} (150 W kg^{-1}) and 99.22 W h kg^{-1} (200 W kg^{-1}).

2.1.5 Starch and cyclodextrin. Starch, the product of photosynthesis in plants, is a natural polysaccharide formed by the polymerization of α-D-glucans. Starch has a high yield after carbonization and is a preferable choice to produce oxygen-rich porous carbon materials[63] Yuan *et al.* obtained hierarchical porous carbon microspheres (HPCMSs) exhibiting large SSA (1668 m^2 g^{-1}), nano-sphericity (4–20 nm) and high carbon content (95%) using starch as the precursor and $K_2C_2O_4$ with $CaCl_2$ as the green activators (Fig. 6a).[64] The HPCMSs achieved a high capacitance (286 F g^{-1}/17.1 μF cm^{-2} at 0.5 A g^{-1}). Furthermore, an outstanding retention of 98% was developed over 20 000 cycles.

What's more, the electrochemical properties of starch-based hierarchical porous carbon (HPC) can be optimized after the pretreatment of starch. Zhao *et al.* obtained HPC with moderate SSA (1863 m^2 g^{-1}) using α-starch from gelatinized starch as the precursor, resulting in a higher capacitance of 335.6 F g^{-1} in comparison with untreated starch.[65] Inspired by the phenomenon of starch turning blue when exposed to iodine, Luo's group prepared a porous iodine-doped carbon skeleton (I-PCs-X) by utilizing the reaction of starch with tartaric acid, potassium nitrate (KNO_3) and iodine to generate the hierarchical porous structure (Fig. 6b).[66] The assembled SSCs with $BiBr_3$ as the electrolyte achieved a superior capacity of 1216 F g^{-1} at 2 A g^{-1} with remarkable energy density (65.4 W h kg^{-1} at 787.3 W kg^{-1}).

Cyclodextrins (CDs), derived from starch hydrolysis, have also been reported as precursors for carbon electrodes. The structure of CDs is a hollow ring, and the three most studied types are α, β and γ, containing 6–8 glucose units respectively. Nowadays, the research on the application of CDs in SCs mainly focuses on its host–guest combination properties.[67–69] Jeong *et al.* combined β-CD with Mn^{2+} and obtained carbon nanofiber (CNF)/MnO_2 composites (PMnCD(β)) by electrostatic spinning and carbonization (Fig. 6c).[67] The PMnCD(β) displayed

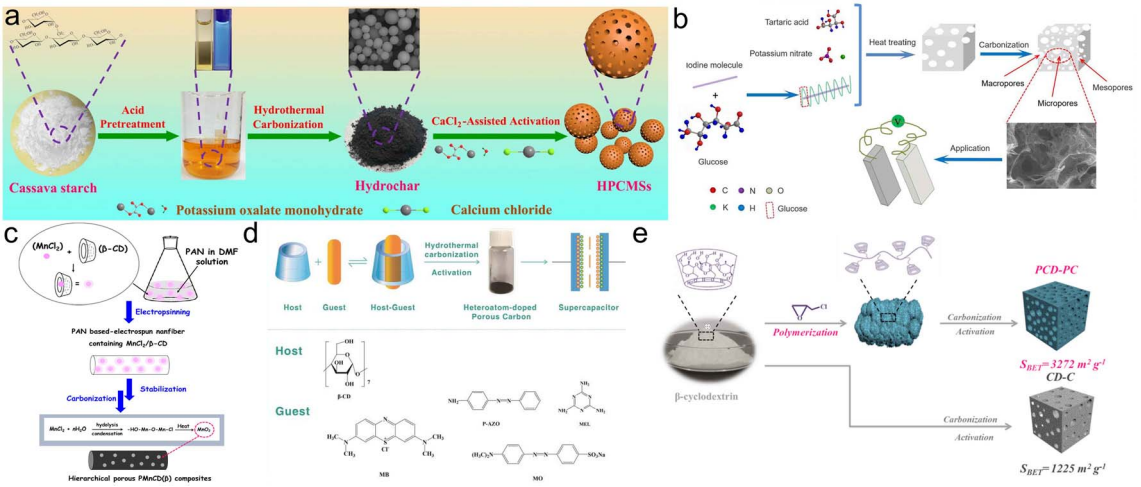

Fig. 6 (a) Illustration for the synthesis of HPCMSs;[64] (b) scheme for the preparation of I-PCs-X;[66] (c) diagram for the construction of PMnCD(β);[67] (d) schematic for the preparation mechanism of porous CMs;[68] (e) mechanism diagram for the synthesis of the PCD-PC.[69]

a moderate capacity of 228 F g^{-1} at 1 mA cm^{-2} with considerable cyclability, thanks to the fast diffusion channels provided by the mesopores of PMnCD(β) and additional pseudocapacitance from N-doping. Chen's group fabricated N, S co-doped carbon materials (CMs) using hydrothermal carbonization followed by KOH activation owing to the coordination of β-CD with guest molecules (Fig. 6d).[68] The CMs delivered a gravimetric capacity of 291.5 F g^{-1} at 0.5 A g^{-1} while achieving well mechanical stability of 94% retention over 10 000 cycles. Meanwhile, cyclodextrin polymers have also been reported as precursors. Lin' group polymerized β-CD and then obtained HPC with ultrahigh SSA of 3710 m^2 g^{-1} (PCD-PC) using the carbonization-activation process (Fig. 6e),[69] which achieved excellent capacity (416 F g^{-1} at 0.5 A g^{-1}).

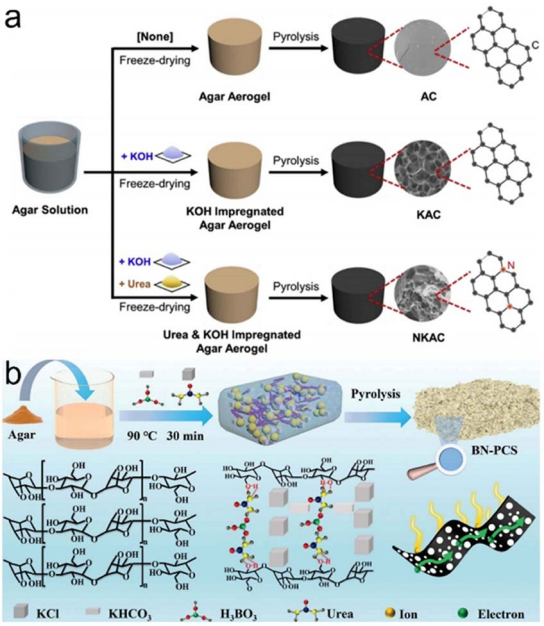

Fig. 7 (a) Diagram for the fabrication of NKAC;[71] (b) schematic for the preparation of BN-PCS.[72]

2.1.6 Agar. Agar, the mixture of agarose and agaropectin derived from red algae, is famous for its room-temperature gelation properties.[70] Zhang's group synthesized N-doped porous carbon aerogels (NKAC) possessing high SSA and small mesoporous structure by pyrolysis with urea as a nitrogen dopant and KOH as an activator based on the self-gelling of agar (Fig. 7a).[71] The NKAC delivered a high capacitance (366.9 F g^{-1} at 0.5 A g^{-1}) with a retention rate of 61.7% at 50 A g^{-1} and favorable cycle stability (96.4% over 10 000 cycles). Liu and coworkers successfully constructed B, N co-doped porous carbon sheets (BN-PCS) derived from agar in the KCl/$KHCO_3$ molten salt system (Fig. 7b).[72] Urea was not only the dopant but also the guiding agent for the two-dimensional (2D) sheet structure during carbonization, while the decomposition of $KHCO_3$ and H_3BO_4 contributed to forming porous structures. The BN-PCS achieved a capacity of 361.1 F g^{-1} at 0.5 A g^{-1} in 6 M KOH, and the corresponding SSC reached a favorable energy density of 43.5 W h kg^{-1} at 375 W kg^{-1} in 1 M $TEABF_4$ in Acetonitrile.

2.2 Protein

2.2.1 Collagen. Collagen is a type of protein with a helical structure, mainly consisting of glycine, proline and hydroxyproline, which exists in bones, skin and carp scales.[73] Collagen serves as a promising precursor for heteroatom doping. Furthermore, collagen aids in the formation of the extracellular matrix, resulting in increased surface area.[74] These properties make it show potential as carbon electrodes. The graphene-based porous carbon (CSGC) doped with N and O atoms was synthesized by Lin and colleagues, who used carp scales as the precursor (Fig. 8a).[75] The CSGC-700 activated at 700 °C exhibited a hybrid structure of graphene layers and amorphous carbon, coordinated with N, O doping, making the ZIHCs assembled with CSGC-700 realize a superior capacity of 138.8 mA h g^{-1}, as

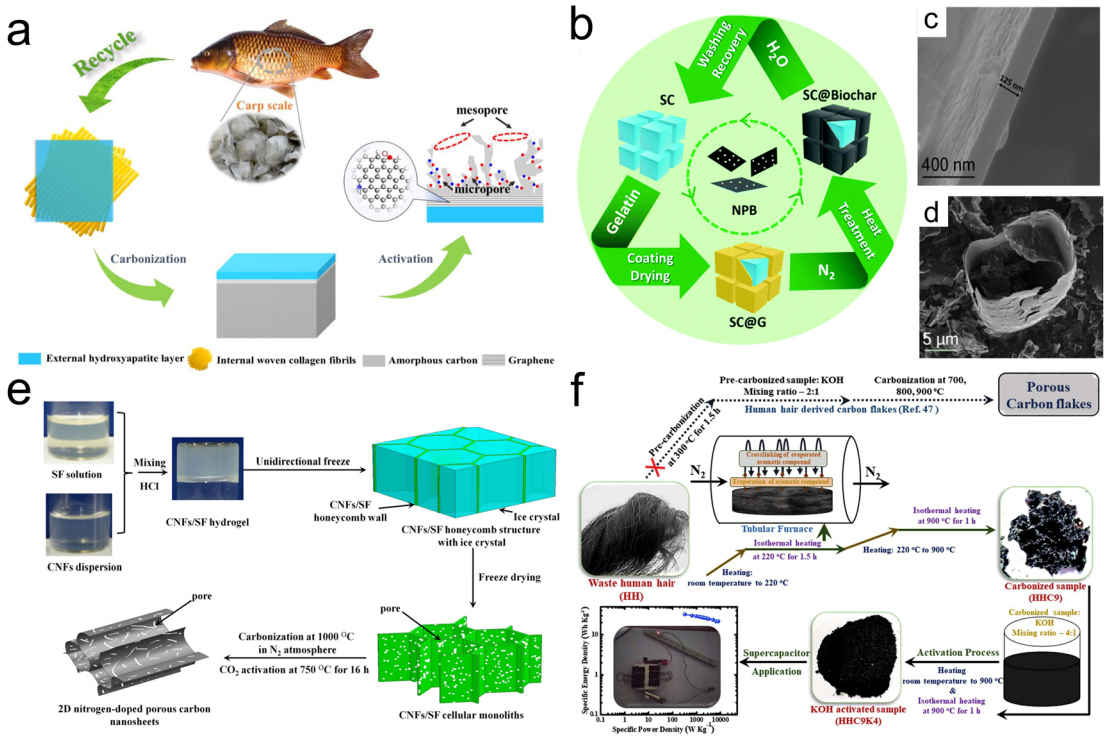

Fig. 8 (a) Scheme for the fabrication of CSGC;[75] (b–d) diagram for the synthesis and SEM images for NPB.[81] (e) diagrams for the fabrication of NPCN;[84] (f) synthetic route for the synthesis of HHC9K4.[88]

well as durable cyclability and outstanding energy density. Subhani *et al.* fabricated graphene-integrated porous carbon aerogel (C-G-collagen) using collagen extracted from chicken feet as the precursor.[76] Benefiting from the porous structure, moderate SSA (1087 m^2 g^{-1}) and interaction of porous carbon and graphene, C-G-collagen demonstrated excellent properties, achieving a remarkable capacitance (365 F g^{-1} at 1 mV s^{-1}) and retention rate of 97% over 10 000 cycles.

2.2.2 Gelatin. Gelatin is the hydrolysis product of collagen. As a mixture of proteins and peptides, gelatin with a high nitrogen content (~16%) can be converted to nitrogen-doped carbon.[77] Gelatin is a kind of hydrophilic colloid with gelation properties forming honeycomb porous carbon.[78] Du *et al.* formed hydrogels by self-assembling the hydrophilic polymer polyacrylamide/gelatin/F127 and prepared 3D layered porous carbon (HPC) by freeze-drying and one-step activation.[79] The mesoporous/microporous ratio and SSA of HPC varied with the amount of KOH. The HPC-3.5 based SSCs (the amount of KOH was 3.5 g) delivered the best electrochemical performance in ionic liquids ($EMIMBF_4$) with an extensive voltage of 3.8 V, outstanding capacity of 216.5 F g^{-1} and superior energy density of 108.6 W h kg^{-1}.

Additionally, gelatin can form carbon nanosheets after carbonization with the assistance of the template.[80] Zhang's group put forward a scalable approach for fabricating N-doped carbon nanosheets, choosing gelatin as the precursor with NaCl as the pyrogenic agent and 2D structure guide (Fig. 8b–d).[81] The optimal sample showed a rich pore structure, highly graphitic and abundant nitrogen content, so beneficial rate performance of 70% retention rate from 0.1 to 20 A g^{-1} and considerable cycle performance (97.4% over 10 000 cycles) were developed.

2.2.3 Fibroin. Fibroin, extracted from silkworm silk, is mainly composed of glycine and alanine with serine, which are ideal nitrogen-rich doping precursors.[82] Sun *et al.* introduced a simple approach to augment the ionic conductivity of N-doped porous carbon (NPC) obtained from silk *via* organic liquid treatment.[83] With the cooperation of organic liquid, the NPC realized an increased capacity (565.3 F g^{-1} at 1 A g^{-1}), and assembled SSCs showcased favorable stability (93.3% over 10 000 cycles) while maintaining an impressive energy density (26.2 W h kg^{-1} at 263.9 W kg^{-1}). Fibroin can transform into different kinds of carbon material with high-temperature treatment thanks to the easy processing. Gao and coworkers developed nitrogen-doped porous carbon nanosheets (NPCN) from CNF/fibroin hydrogel *via* freeze-drying, carbonization and CO_2 activation (Fig. 8e).[84] The NPCN-50 (the mass ratio of fibroin to CNF was 50 : 50) showed a high capacity (329.9 F g^{-1} at 0.25 A g^{-1}) with an excellent retention rate of 99.5% over 5000 cycles owing to 2D nanostructure, abundant pore distribution, high SSA and heteroatom doping.

2.2.4 Keratin. Keratin, consisting of dead cells produced by biological systems, is the main protein that makes up the outer layer of hair, feathers, horns, claws, and human skin.[85] Keratin consists of various amino acids such as threonine, cysteine, histidine and methionine, and is rich in C, O, N and S, which is a promising precursor for heteroatom doping.[86] Wu and coworkers developed N, O and S co-doped HPC, choosing keratin derived from chicken feathers.[87] The optimal sample

exhibited a total porosity volume of 1.461 $m^3 g^{-1}$ and elevated SSA of 2864 $m^2 g^{-1}$, thus culminating in a nice capacity (270 F g^{-1} at 1 A g^{-1}) with favorable stability (98% over 10 000 cycles). Sinha and coworkers used keratin extracted from waste hair as a carbon source and introduced a low-temperature section (220 °C, 1.5 h) into the carbonization to prevent the evaporation of volatile molecules and to facilitate the rearrangement of heteroatoms (Fig. 8f).[88] Due to the interlinked porous nanosheet structure and rich heteroatom content, the electrodes of KOH-activated carbon material (HHC9K4) manifested an ultrahigh capacity (999 F g^{-1} at 1 A g^{-1}), and corresponding SSCs attained a remarkable energy density of 32 W h kg^{-1} at 324 W kg^{-1}.

3. Strategies for boosting the capacitance of biopolymers-based electrodes

As the most prevalent electrode materials utilized in SCs, carbon materials derived from biopolymers show favorable cycling stability and high power density, but poor capacity limits their further applications.[89] Various methods have been proposed to solve this problem, which can be summarized in the following three directions: (a) pore engineering, (b) doping engineering and (c) composite engineering. These strategies will be discussed in this part.

3.1 Pore engineering

It is well known that a reasonable pore size distribution (PSD) is in favor of carbon materials exhibiting promising capacitance and rate properties.[90] Due to the dissolution of electrolyte ions, micropores (<2 nm) can increase the SSA, thus improving the capacitance,[91] but excessive micropores result in slow ion transport kinetics and high resistance leading to poor rate performance.[92] Mesopores (2–50 nm) can offer diffusion pathways for ions, improve electrolyte wetting, promote ion diffusion and ensure well-rate performance and power density.[93] Macropores (>50 nm), as the ion buffers, can store electrolytes and shorten the diffusion distance of ions.[90,94]

Generally, biopolymers require a pyrolysis-activation process to transform into carbon-based electrodes. Carbonization can be carried out in two routes: (a) pyrolysis, which is a high-temperature reaction (500–1000 °C) in an inert atmosphere; (b) hydrothermal carbonization (HTC) is a high-pressure thermal reaction at low temperatures (<250 °C). However, biopolymer carbonization products exhibit a low SSA and underdeveloped pores, requiring further activation.[95]

3.1.1 Activation. Based on the different reaction mechanisms, the activation method can be categorized into physical, chemical and biological activation. Physical activation, also known as "thermal activation", is a reaction of high-temperature gases (*e.g.* CO_2, air, steam, *etc.*) with biopolymers to obtain pore formation.[96,97] Physical activation is more beneficial to the environment, but the resulting activated carbon has a low yield, narrow PSD and low SSA, making its specific capacitance difficult to meet realistic conditions.[12,98] So it is less studied and usually used in conjunction with chemical activation.

Chemical activation utilizes the chemical reaction between the activator and carbonization product or biopolymers to achieve pore formation.[99] Depending on the type of activator, chemical activation is distinguished by alkali, acid and salt activation.[100] KOH is the most popular alkali activator for obtaining carbon materials with large SSA and relatively uniform PSD, and the reaction mechanism of KOH is shown in eqn (1)–(5). Meng *et al.* combined chitosan aerogels with KOH to obtain mesoporous-dominated N, O co-doped porous carbon (HPC) using freeze-drying and one-step activation (Fig. 9a).[99] The HPC exhibited the maximum SSA of 2787.47 $m^2 g^{-1}$, thus delivering a favorable capacity of 253 F g^{-1} at 0.5 A g^{-1}.

$$2C + 6KOH \rightarrow 2K + 2K_2CO_3 + 3H_2 \quad (1)$$

$$2C + K_2CO_3 \rightarrow 3CO + 2K \quad (2)$$

$$K_2CO_3 \rightarrow CO_2 + 2K \quad (3)$$

$$C + K_2O \rightarrow CO + 2K \quad (4)$$

$$C + CO_2 \rightarrow 2CO \quad (5)$$

As a typical acid activator, phosphoric acid (H_3PO_4) activation consists of five steps: hydrolyzation, dehydration, aromatization, cross-linking and pore creation.[101] Cao *et al.* used H_3PO_4 to dehydrate lignin and alleviate the hydrogen bonding between lignin molecules to obtain phosphorylated lignin, which subsequently reacted with cellulose acetate (CA) hydroxyl groups to form phospholipid bonds, reducing the phase separation of CA from lignin and enhancing the thermal stability of the precursor fiber.[102] After a simple pre-oxidation, the obtained carbon fibers (CFs) developed a remarkable capacitance of 346.6 F g^{-1}.

Zinc chloride ($ZnCl_2$) is a commonly used salt activator offering both dehydration and deoxygenation during the activation process.[103] Yang *et al.* utilized cellulose-rich cotton pulp paper as the precursor and prepared cellulose-derived carbon (CDC) possessing enriched meso- and micro-pores by a one-step $ZnCl_2$ activation (Fig. 9b).[104] The solid-state ZIHCs with CDC as the cathode yielded an excellent capacity of 247 mA h g^{-1} and energy density of 243 W h kg^{-1} while upholding a decent retention rate of 85% over 20 000 cycles. Zhai's group used chitin as the precursor and $ZnCl_2$ as the dehydrator and activator to deliver N-doped carbon aerogels (NSCA) with a maximum SSA of 2540 $m^2 g^{-1}$.[105] The NSCA-1000 carbonized at 1000 °C exhibited a favorable capacity of 249.4 F g^{-1} at 1 A g^{-1}. Furthermore, even after undergoing 15 000 cycles, a retention rate of 98.44% was obtained.

Considering the environmental hazards of conventional activators and the cumbersome synthesis process of activated carbon, alternative salt activators have been tried with success. Depending on the activation mechanism, they are classified into three categories: molten salts (NaCl, KCl, LiCl, *etc.*), decomposition salts ($KHCO_3$, $NaNO_3$, $Zn(Ac)_2$, *etc.*), and

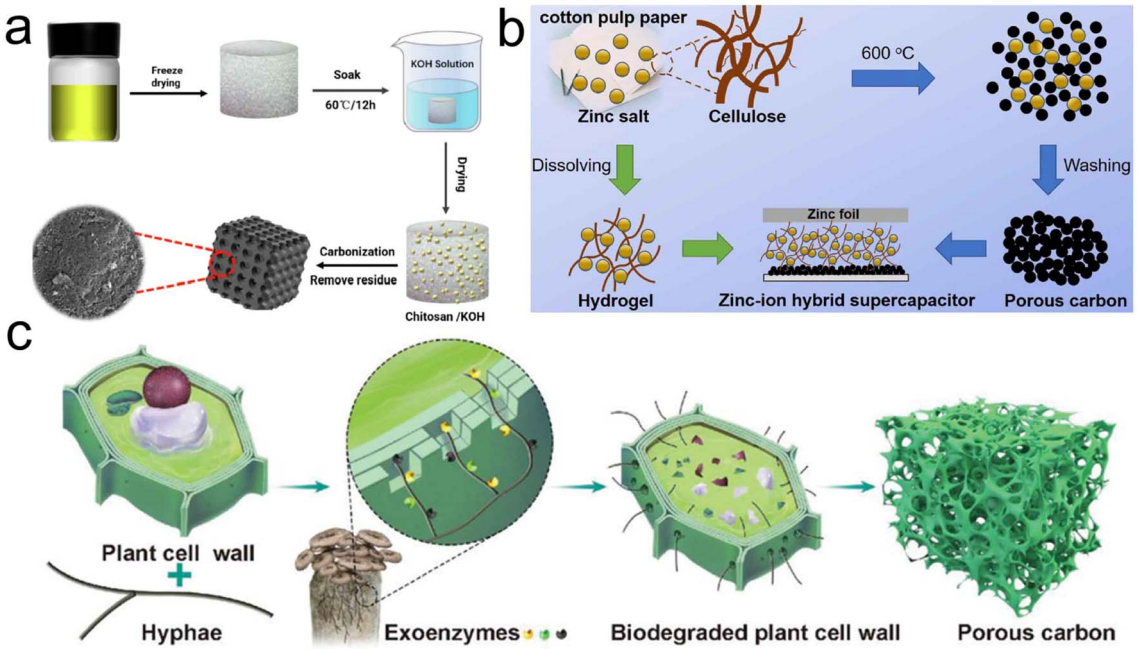

Fig. 9 (a) Fabrication schematic for the HPC-X;[99] (b) scheme of design for the ZIHS by using CDC as the cathode and cellulose hydrogel containing $ZnCl_2$ as the electrolyte;[104] (c) schematic diagram of fungi-enabled degradation of the plant cell wall to obtain porous carbon with ultrahigh SSA.[113]

oxidation salts (HNO_3, $KMnO_4$, K_2FeO_4, *etc.*).[106–108] Being a green activator, the molten salt can be easily removed after the carbonization without the need for acid washing. Wang and colleagues developed a lignin-based nitrogen-doped hierarchically porous carbon (LDMCN-700-2) by one-step activation using KCl as the activator and hard template, exhibiting a moderate SSA (1012.5 $m^2\ g^{-1}$) with notable nitrogen content (4.5 at%). So favorable properties, such as high capacitance (245 $F\ g^{-1}$ at 0.5 $A\ g^{-1}$) and favorable mechanical stability (95.7% upon undergoing 5000 cycles) were achieved.[109] The gas generated by the reaction of decomposing salts can etch the carbon matrix to form pores. Deng *et al.* were inspired by bread fermentation and proposed a strategy of $KHCO_3$-assisted pyrolysis to obtain micro- and mesopores, while the CO_2 produced by $KHCO_3$ decomposition expanded and produced macropores, resulting in an HPC with high SSA (1893 $m^2\ g^{-1}$). Consequently, it exhibited remarkable capacity (253 $F\ g^{-1}$), along with low resistance and durable stability.[110] In addition, oxidation salts can act as both activators and templates. Wang *et al.* chose chitin as the precursor and $KMnO_4$ as the activator for generating micropores and small mesopores, while the generated K_2MnO_4 and MnO_2 could be acted as templates to generate meso- and macropores.[111] The obtained carbon material of HPC-700 could reach a substantial pore volume (1.286 $cm^3\ g^{-1}$) with high SSA (1488.3 $m^2\ g^{-1}$), demonstrating a significant capacity (412.5 $F\ g^{-1}$ at 0.5 $A\ g^{-1}$).

Biological activation is the use of microorganisms to degrade biopolymers, thereby achieving pore creation.[112–114] Wang *et al.* first introduced the strategy for preparing porous carbon *via* fungal degradation of lignin (Fig. 9c).[113] The structure of cotton seed hulls was embrittled by exoenzymes after inoculation with Pleurotus ostreatus. A 3D loose precursor of the honeycomb-like structure was formed, which could facilitate matrix carbonization and KOH activation to form abundant pores. The assembled lithium-ion capacitors demonstrated an ultrahigh energy density of 263.9 $W\ h\ kg^{-1}$ at 0.7 $kW\ kg^{-1}$. Samely, Wang's group exploited cellulase to degrade cellulose in wood, followed by high-temperature carbonization to obtain self-supported thick carbon electrodes possessing high SSA and hierarchically arranged porous structures, thus realizing the gravimetric capacitance of 384 $F\ g^{-1}$ and volume capacitance of 8.41 $F\ cm^{-2}$ at 1 $mA\ cm^{-2}$.[114]

3.1.2 Template. The template method primarily employs three kinds of templates: hard templates, soft templates and self-templates. As for the synthesis of HPC with hard templates, biopolymers need to combine with the hard template, and then porous carbon is obtained after a high-temperature reaction and template removal.[115] In addition to the molten salts, commonly employed hard templates include silica-based templates (*e.g.*, mesoporous SiO_2, tetraethyl silicate, *etc.*), metal oxides (*e.g.*, ZnO, MgO, CaO, *etc.*) and ice templates.[116–120] Cao *et al.* synthesized HPC with high SSA and controlled porosity using exothermic pyrolysis of starch with magnesium nitrate and subsequent heat treatment and acid washing (Fig. 10a).[119] The optimized sample showed a hierarchical porous network with an SSA of 2200 $m^2\ g^{-1}$ that offered accessible pathways for electrolyte transport, demonstrating the well electrochemical properties with moderate specific capacity (229 $F\ g^{-1}$ at 1 $A\ g^{-1}$), outstanding rate capability (92.13% retention to 10 $A\ g^{-1}$) and decent cyclability (94% over 10 000 cycles). Liu's group obtained silicate/chitosan microspheres (PBE) by spray drying using SiO_2 as the mesoporous template.[121] The regular

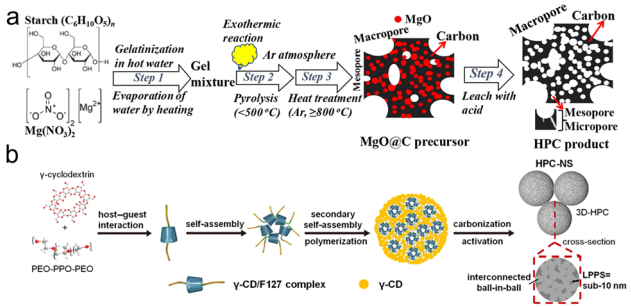

Fig. 10 (a) Diagram for the fabrication of HPC;[119] (b) scheme for the formation mechanism of HPC-NS.[126]

honeycomb-like HPC was obtained by one-pot carbonization using polytetrafluoroethylene as an etching agent and macroporous guide. The SSCs assembled with PBE exhibited a beneficial capacitance (250.5 F g^{-1} at 0.5 A g^{-1}) and an excellent retention rate of up to 107% over 5000 cycles.

Organic molecules or block copolymers with functional groups often act as soft templates.[122–125] In a suitable solvent, the soft templates self-assemble into micelles to bond with the biopolymer through interactions to form a coating of encapsulated carbon precursors. Finally, the micelles decompose to obtain porous carbon during carbonization. Yao and coworkers developed hierarchically porous carbon nanospheres (HPC-NS) with interlinked ball-in-ball structures using pyrolysis of γ-CD/F127 (Fig. 10b).[126] The connectivity of the pores facilitated ion transport, enabling excellent electrochemical properties, allowing for 405 F g^{-1} specific capacity at 1 A g^{-1} with a retention of 71% to 200 A g^{-1}. Moreover, an impressive energy density of 24.3 W h kg^{-1} was achieved at 151 W kg^{-1}. Ionic liquid (IL) as soft templates have also been reported. Using chitosan as the precursor and IL (2-butyl-1-methylimidazolium chloride) as the soft template, Wu *et al.* synthesized 2D layered graphitized carbon (NCSIL-900) with micro- and mesoporous structures by a one-pot hydrothermal, thus achieving the capacity of 355 F g^{-1} in 1 M H_2SO_4 and 275 F g^{-1} in 6 M KOH.[127]

Anionic polymers (*e.g.*, lignosulfonates, alginates, *etc.*) can act as self-templates by generating metal compounds through pyrolysis without the introduction of additional templates, resulting in pores.[128–130] Pang *et al.* chose SLS as the carbon source to fabricate SLS-derived HPC by carbonization without adding an extra template.[131] The porous carbon (HPCSLS-700-1) showed the maximum SSA of 903 m^2 g^{-1} and notable heteroatom contents (O 8.11 at%, N 1.76 at%). The SSCs assembled with HPCSLS-700-1 in 7 M KOH demonstrated a decent capacity of 247 F g^{-1} with a remarkable retention of 92% over 20 000 cycles.

3.2 Doping engineering

As another strategy for improving the capacity for carbon electrodes, heteroatom doping can be classified into two kinds: *in situ* and *ex situ* doping, where the former involves the calcination of precursors containing heteroatoms and the latter involves the introduction of heteroatoms through dopants.[132,133] Moreover, depending on the kinds of dopant atoms, heteroatom doping can be classified as single and multiple heteroatom co-doping.[134] Introducing heteroatoms not only augments the conductivity of carbon-based electrodes but also enhances the wettability in the electrolyte. More importantly, heteroatom doping provides pseudocapacitance and promotes hybrid capacitance.[135]

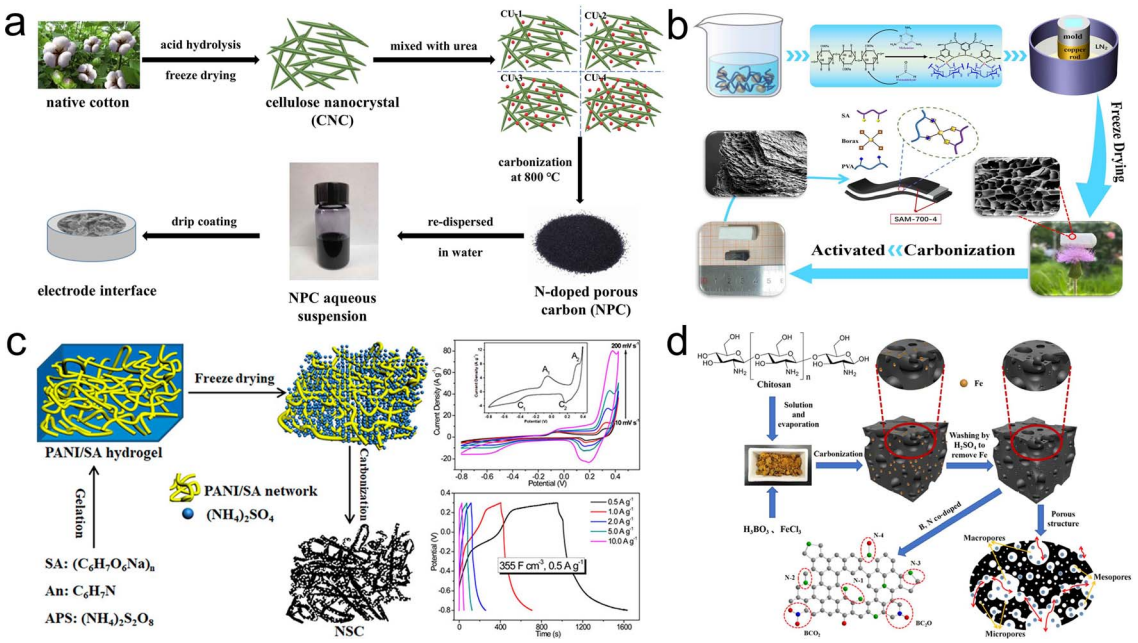

Fig. 11 (a) Scheme for preparation of the NPC based on CNC and urea;[139] (b) schematic for the synthesis of SAM-700-4;[140] (c) illustration for fabrication procedure of NSC;[145] (d) schematic diagram of the synthesis of BNPC-Fe.[147]

3.2.1 Single heteroatom doping. Nitrogen atoms are one of the most common dopant atoms, which easily bind to the carbon framework because their radius is comparable to the carbon atom.[136] Nitrogen-doped carbon structures contain four types of functional groups: pyridine nitrogen (N-6), pyrroline nitrogen (N-5), quaternary nitrogen (N-Q) and oxidized nitrogen (N–O), where N-5 and N-6 offer active sites for Faraday reactions, while N-Q and N–O lead to electron transport.[137,138] Wang and colleagues fabricated N-doped porous carbon (NPC) possessing moderate SSA (366.5 m^2 g^{-1}) with rich nitrogen content (7.4 at%), who used CNCs as the precursor with urea as the dopant (Fig. 11a).[139] So the NPC achieved ultrahigh capacitance (570.6 F g^{-1} at 1 A g^{-1}). Sun's group delivered N-doped carbon aerogels from SA/melamine composites (SAM) in Fig. 11b.[140] Benefiting from its high heteroatom content, large SSA and unique directional channel structure, the SAM-700-4, synthesized at an optimal carbonization temperature of 700 °C and with a KOH/SAM ratio of 4, demonstrated an excellent capacity (441.80 F g^{-1} at 0.5 A g^{-1}).

Doping of phosphorus and sulfur atoms with larger radii and higher electrochemical activities introduces greater structural distortions and defects to the carbon skeleton compared with nitrogen doping.[141,142] Boron and nitrogen atoms have a comparable radius to carbon atoms, making boron atoms easier to incorporate into carbon compounds. Boron doping increases the concentration of carrier holes, resulting in p-type doping and increased electrical conductivity.[143] However, single phosphorus, sulfur, and boron atom doping are seldom reported, which is attributed to the low doping content making it difficult to effectively enhance the electrochemical properties, and hence co-doping tends to be done in collaboration with the nitrogen atom. Furthermore, it is a controversial topic whether oxygen is the doping atom or not. The functional groups containing oxygen, such as carboxy, carbonyl and hydroxy, can participate in Faraday reactions and improve the capacitance of aqueous SCs.[134] However, it is undeniable that the majority of carbon electrodes contain oxygen and the content is not low, so it will not be discussed here.

3.2.2 Multiple heteroatom doping. Recently, more studies have proved that the synergistic effect of heteroatom co-doping contributes to boosting the performance of SCs. The surface condition and electronic property of carbon materials are more active thanks to introducing more heteroatoms, which facilitates exposure to more active sites for charge storage.[144] Considering a large amount of co-doping types, this part will focus on the more frequently used "N + X" doping (X = B, P, S, *etc.*).

As for N, S co-doping, introducing nitrogen and sulfur atoms enhances the hybrid capacitance while increasing the conductivity and carbon layer spacing.[137] Huang's group fabricated micropore-dominated N, S co-doped carbon (NSC) based on the interaction between PANI and SA followed by one-step carbonization (Fig. 11c).[145] The authors used ammonium sulfate, which was the by-product of aniline polymerization, as the nitrogen, sulfur activator to introduce N, S doping while optimizing the carbon structure. Thanks to the N, S co-doping with hierarchical porous structure, the NSC exhibited pseudocapacitive properties with high bulk capacity (355 F cm^{-3} at 0.5 A g^{-1}), and the assembled SSC achieved excellent energy density (15.9 W h L^{-1} at 426 W L^{-1}). Particularly, N, P co-doping helps to extend the voltage window in aqueous electrolytes while generating pseudocapacitance. Fan's group developed the porous carbon doped with N, P atoms (APC) from hydrogels formed by the interaction of chitosan with phytic acid.[146] The optimized APC-2 showed a hierarchically porous framework, high SSA and an abundance of heteroatom. Thus, the voltages of corresponding SSCs were up to 1.3 V (6 M KOH) and 1.7 V (1 M Na_2SO_4). Nitrogen and boron atoms are electron-rich and electron-deficient, respectively. The B, N co-doping can produce special electronic structures to improve the electrochemical performance. Qiu's group used chitosan as a precursor, boric acid as a template and boron source and ferric chloride as a multifunctional reagent (solvent, template and activator) to prepare B, N co-doped porous carbon (BNPC-Fe) in Fig. 11d.[147] The BNPC-Fe delivered an increased capacitance (348 F g^{-1} at 1 A g^{-1}) compared to NPC-Fe without boric acid added.

3.3 Composite engineering

In addition to pore and doping engineering, combining biopolymers-based carbon materials with other carbon materials, transition metal compounds and conductive polymers utilizes the synergistic interplay of these constituents to form composites with multi-component, hierarchical structures and abundant active sites to achieve optimum electrochemical performance.

3.3.1 Carbon/carbon composite. Biopolymers-based porous carbon typically has an amorphous structure, resulting in poor conductivity and restricting rate performance. Carbon nanomaterials (*e.g.* graphene, carbon nanotubes and Mxene) generally deliver excellent conductivity and relatively high capacity, but the stacking of carbon nanomaterials limits ion dynamics and active site exposure.[148] Combining porous carbon with carbon nanomaterials can help to solve the above problems and thus enhance the performance of the composite. Ma's group constructed the nitrogen, sulfur co-doped porous carbon foam reinforced by graphene (N, S-GHPCF) using sol–gel and one-step carbonization.[149] The samples showed an amplified SSA (2279.2 m^2 g^{-1}), well conductivity (438 S m^{-1}) and rich heteroatom content, realizing ultrahigh capacitance (405 F g^{-1} at 1 A g^{-1}), along with impressive rate capability (72.8% retention to 100 A g^{-1}) and cycle stability (98.8% over 10 000 cycles). To solve the problem with the stacking of MXene, Zhang and coworkers introduced a strategy of carbon dots intercalation to prepare flexible MXene thin film electrodes of high ion-accessible surface and large density *via* gelatin of calcium alginate with MXene and carbonization (Fig. 12a and b).[150] The electrodes demonstrated superior capacitance (372.6 F g^{-1} and 1244.6 F cm^{-3} at 1 A g^{-1}) coupled with outstanding rate performance (198.3 F g^{-1} and 662.5 F cm^{-3} to 1000 A g^{-1}) and cycle stability (93.5% retention over 30 000 times).

3.3.2 Carbon/transition metal compounds. As promising pseudocapacitive materials, transition metal compounds

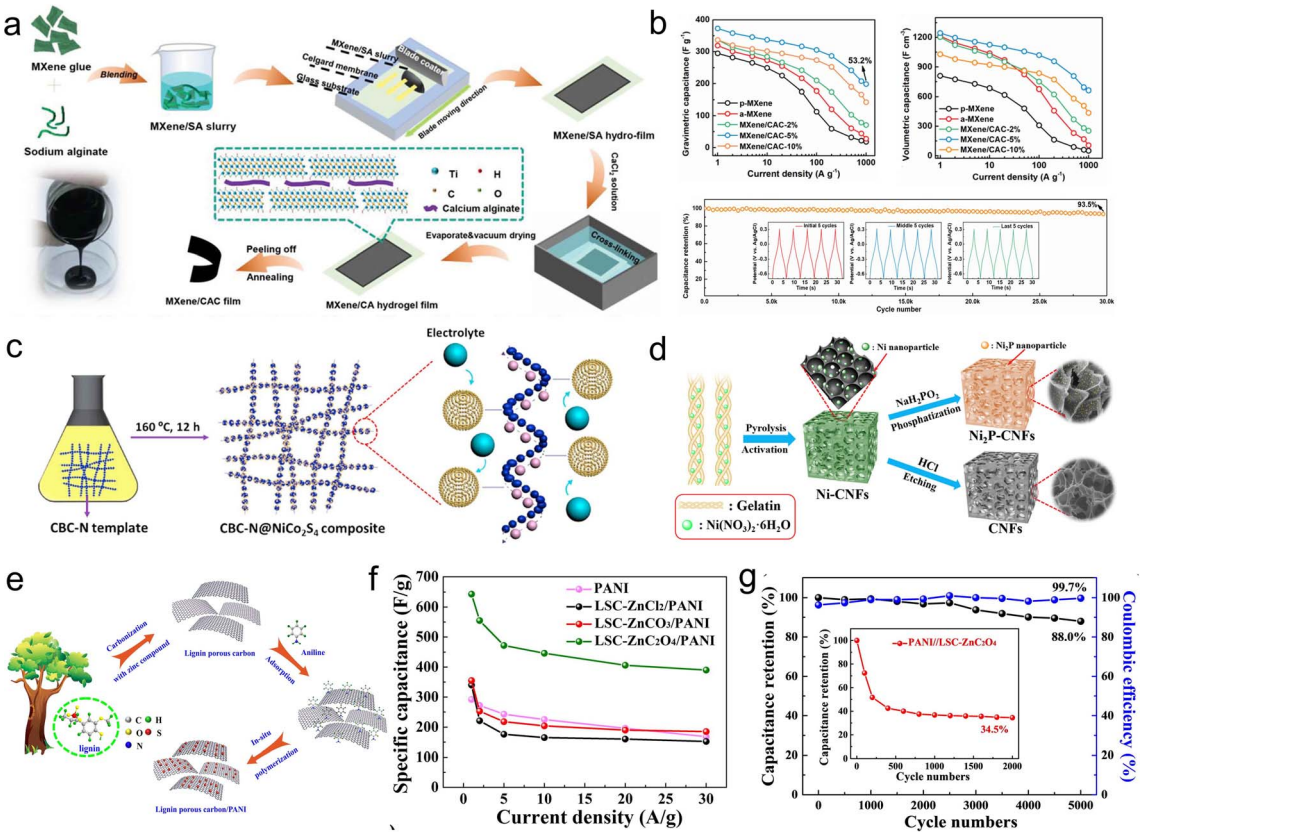

Fig. 12 (a) Scheme for the synthesis of MXene/CAC films; (b) capacity and cycling stability test of MXene/CAC;[150] (c) scheme for the space-confined growth of CBC-N@$NiCo_2S_4$ composite;[155] (d) diagrams for the preparation of Ni-CNFs, Ni_2P-CNFs and CNFs;[156] (e) schematic for the fabrication of lignin porous carbon/PANI composites; (f) specific capacitance of the samples; (g) cycling test of LSC-ZnC_2O_4/PANI//LSC-ZnC_2O_4 ASCs.[161]

(TMCs) can provide high capacitance and store much energy through reversible faradaic reactions.[151] However, the volume variation induced by the phase change during the reaction leads to undesirable reaction kinetics and cycling stability.[152] The integration of TMCs with biopolymers-derived porous carbon composites serves to optimize the conductivity of TMCs, alleviate volume fluctuations and prevent aggregation. Furthermore, it enhances the capacitance of carbon-based electrodes, thereby yielding increased energy density.[153] Zhao's group fabricated chitosan-based hierarchical porous carbon aerogel (HPCA) *via* carbonization and activation followed by anchoring NiCo-LDH nanosheets upon the HPCA using hydrothermal reaction.[154] Thanks to the interaction of HPCA and NiCo-LDHs, the optimized sample exhibited a superior specific capacity (1504 F g^{-1} at 1 A g^{-1}), still retaining the value of 1219.7 F g^{-1} at 10 A g^{-1}. After 5000 cycles, a capacity retention of 86% was identified. Ning and coworkers anchored $NiCo_2S_4$ nanoparticles on the N-doped carbon nanofibers (CBC-N) through the hydrothermal method (Fig. 12c).[155] The CBC-N@$NiCo_2S_4$ composites exhibited a 3D conductive network, realizing an ultrahigh capacity (1078 F g^{-1} at 1 A g^{-1}) and excellent stability (94.6% over 5000 cycling times) than $NiCo_2S_4$. Peng *et al.* achieved Ni_2P nanoparticles dispersing in carbon nanosheet framework (Ni_2P-CNFs) through $Ni(NO_3)_2$-assisted gelatin carbonization with a low-temperature phosphating process (Fig. 12d).[156] The CNFs provided conductive accesses and inhibited the aggregation of Ni_2P nanoparticles, so Ni_2P-CNFs showed a decent capacity (145 mA h g^{-1} at 0.5 A g^{-1}), and assembled Ni_2P-CNFs//CNFs ASCs gave the voltage window up to 1.65 V and maximum energy density of 42 W h kg^{-1} at 413 W kg^{-1}. Additionally, a remarkable capacity retention of 88% upon undergoing 6000 cycling times was realized.

3.3.3 Carbon/conductive polymers. As another kind of PCs' material, conductive polymers (CPs) conduct electricity through conjugated π bonds in polymer chains.[22] The CPs are difficult to achieve excellent electrochemical performance owing to the limitations of self-aggregation, high transport resistance and volume change.[157] So it is necessary to combine CPs with biopolymers-based porous carbon to improve the spatial structure and conductivity of CPs.[158] Zhuo *et al.* loaded PPy uniformly on the cellulose-derived carbon aerogel (Cell@PPy), which achieved an increased capacitance (387.6 F g^{-1} at 0.5 A g^{-1}).[159] Meanwhile, the cell's porous structure effectively promotes the cycling stability of PPy, so the retention of 92.6% over 10 000 cycles was obtained. Liu's group constructed the network of carbon nanofiber/carbon nanosheet (CNF/CNS) through the pyrolysis process of BCs and exploited it as the substrate to modify the nanorod array of PANI.[160] The PANI@CNF/CNS exhibited good hydrophilicity and rapid ion diffusion. Based on these advantages, the ASCs which utilized

PANI@CNF/CNS as the positive electrodes and CNF/CNS as the negative electrodes delivered a remarkable energy density (65.3 W h kg^{-1} at 800 W kg^{-1}) with outstanding stability (98% upon undergoing 5000 cycles). Fu and coworkers used SLS as the precursor and selected different activators ($ZnCl_2$, $ZnCO_3$ and ZnC_2O_4) to obtain porous carbons with various structures, and continued to prepare PANI/porous carbon composites by *in situ* polymerization (Fig. 12e).[161] The results showed that the lamellar porous carbon offered a bigger contact area to penetrate and diffuse the aniline molecules, achieving an excellent capacity (643 F g^{-1} at 1 A g^{-1}). The capacity retention of ASCs was as high as 88% after 5000 cycles (Fig. 12f and g).

4. Conclusion and perspective

As an alternative to synthetic polymers, biopolymers have great advantages, such as green environmental protection, abundant reserves and low budget, which contribute to the popularization of SCs as green energy storage devices and achieve sustainable development.[25] This paper has reviewed the recent advances in biopolymers-based carbon electrodes for SCs and summarized the directions to promote the capacitance of carbon electrodes. Although great progress has been made, there are still many challenges that need to be resolved.

4.1 Raw material optimization

The diversity of types and structures of biopolymers makes them less effectively utilized. Moreover, the separation and purification of biopolymer components is also extremely challenging to achieve.

4.2 Tailored optimization of pore and composition

Although several strategies for optimizing the pore structure have been reported, most of the processes are indeterminate and do not allow for tailored pore size distribution. At the same time, activator etching will reduce the heteroatom content, which makes it hard to optimize capacitance. Therefore, optimizing the structure and heteroatom content of carbon-based electrodes will be the major investigation direction for future research.

4.3 Scaleup and green production

Biopolymers-based carbon electrodes with excellent performance reported in the literature are limited to the laboratory level, and the complicated synthesis methods are difficult to achieve popularization, so it is imperative to introduce facile and scalable strategies for production.[24] In addition, the gases from high-temperature reactions may be harmful to the environment and require further treatment to achieve green production.

4.4 Energy density enhancement

The development of SCs is limited by inadequate energy density, which can be optimized through an increased capacitance and wider voltage window.[162] Combining biopolymers-based carbon materials with pseudocapacitive materials is effective in boosting capacitance, but pseudocapacitive materials tend to fall off during repetitive charging and discharging cycles.[163] The utilization of non-aqueous electrolytes contributes to a wider voltage window, but the electrolyte ions need to be compatible with the pore structure to reach their full potential. Hence, exploring the correlation between the structure and electrochemical characteristics of biopolymers-based carbon electrodes holds immense potential as a burgeoning area of research interest in the realm of supercapacitors (SCs).

4.5 Application expansion

Flexible and wearable electronics provide opportunities for supercapacitor development. Biopolymers can be applied as electrodes for flexible and stretchable SCs.[164] However, achieving electrochemical performance comparable to conventional SCs is an urgent issue.

Conflicts of interest

There are no conflicts to declare.

Acknowledgements

The authors gratefully acknowledge the financial support from the National Key Research Development Program of China (2021YFB3800300), and the Open Project of State Key Laboratory of Metal Matrix Composites (2021SKLMMC-8).

References

1 R. P. Rastogi, A. Pandey, C. Larroche and D. Madamwar, *Renewable Sustainable Energy Rev.*, 2018, **82**, 2946–2969.
2 Z. Liu, D. B. Guan, S. Moore, H. Lee, J. Su and Q. Zhang, *Nature*, 2015, **522**, 279–281.
3 F. Biermann, T. Hickmann, C. A. Senit, M. Beisheim, S. Bernstein, P. Chasek, L. Grob, R. E. Kim, L. J. Kotze, M. Nilsson, A. O. Llanos, C. Okereke, P. Pradhan, R. Raven, Y. X. Sun, M. J. Vijge, D. van Vuuren and B. Wicke, *Nat. Sustain.*, 2022, **5**, 795–800.
4 H. Jin, J. Li, Y. Yuan, J. Wang, J. Lu and S. Wang, *Adv. Energy Mater.*, 2018, **8**, 1801007.
5 Y. L. Shao, M. F. El-Kady, J. Y. Sun, Y. G. Li, Q. H. Zhang, M. F. Zhu, H. Z. Wang, B. Dunn and R. B. Kaner, *Chem. Rev.*, 2018, **118**, 9233–9280.
6 E. S. Appiah, P. Dzikunu, N. Mahadeen, D. N. Ampong, K. Mensah-Darkwa, A. Kumar, R. K. Gupta and M. Adom-Asamoah, *Molecules*, 2022, **27**, 6556.
7 F. X. Wang, X. W. Wu, X. H. Yuan, Z. C. Liu, Y. Zhang, L. J. Fu, Y. S. Zhu, Q. M. Zhou, Y. P. Wu and W. Huang, *Chem. Soc. Rev.*, 2017, **46**, 6816–6854.
8 K. F. Chen and D. F. Xue, *J. Mater. Chem. A*, 2016, **4**, 7522–7537.
9 V. Aravindan, J. Gnanaraj, Y. S. Lee and S. Madhavi, *Chem. Rev.*, 2014, **114**, 11619–11635.

10 K. L. Van Aken, M. Beidaghi and Y. Gogotsi, *Angew. Chem. Int. Ed.*, 2015, **54**, 4806–4809.
11 Z. N. Yu, L. Tetard, L. Zhai and J. Thomas, *Energy Environ. Sci.*, 2015, **8**, 702–730.
12 H. Lu and X. S. Zhao, *Sustain. Energy Fuels*, 2017, **1**, 1265–1281.
13 R. Vinodh, Y. Sasikumar, H. J. Kim, R. Atchudan and M. Yi, *J. Ind. Eng. Chem.*, 2021, **104**, 155–171.
14 S. W. Bokhari, A. H. Siddique, H. Pan, Y. Li, M. Imtiaz, Z. Chen, S. M. Zhu and D. Zhang, *RSC Adv.*, 2017, **7**, 18926–18936.
15 M. Shaker, A. A. S. Ghazvini, W. Cao, R. Riahifar and Q. Ge, *New Carbon Mater.*, 2021, **36**, 546–572.
16 C. Choi, D. S. Ashby, D. M. Butts, R. H. DeBlock, Q. L. Wei, J. Lau and B. Dunn, *Nat. Rev. Mater.*, 2020, **5**, 5–19.
17 M. Zenasni, H. Belhadj, M. Kiari, M. Alelyani, A. B. Alhailiy, A. Benyoucef and Y. Bakkour, *Front. Energy Res.*, 2023, **11**, 1244699.
18 Y. Yan, T. Y. Wang, X. R. Li, H. Pang and H. G. Xue, *Inorg. Chem. Front.*, 2017, **4**, 33–51.
19 D. Majumdar, T. Maiyalagan and Z. Q. Jiang, *Chemelectrochem*, 2019, **6**, 4343–4372.
20 S. S. Patil and P. S. Patil, *Nanoscale*, 2022, **14**, 16731–16748.
21 G. F. Xue, T. Bai, W. G. Wang, S. J. Wang and M. D. Ye, *J. Mater. Chem. A*, 2022, **10**, 8087–8106.
22 G. A. Snook, P. Kao and A. S. Best, *J. Power Sources*, 2011, **196**, 1–12.
23 R. Y. N, K. Sharma and P. M. Shafi, *J. Energy Storage*, 2022, **55**, 105727.
24 S. Ahmed, P. Sharma, S. Bairagi, N. P. Rumjit, S. Garg, A. Ali, C. W. Lai, S. M. Mousavi, S. A. Hashemi and C. M. Hussain, *J. Energy Storage*, 2023, **66**, 107391.
25 Y. X. Wang, T. Xu, K. Liu, M. Zhang, X. M. Cai and C. L. Si, *Aggregate*, 2023, e248.
26 N. Boutaleb, F. Z. Dahou, H. Djelad, L. Sabantina, I. Moulefera and A. Benyoucef, *Polymers*, 2022, **14**, 4562.
27 G. Gopinath, S. Ayyasamy, P. Shanmugaraj, R. Swaminathan, K. Subbiah and S. Kandasamy, *J. Energy Storage*, 2023, **70**, 108065.
28 Z. H. Bi, Q. Q. Kong, Y. F. Cao, G. H. Sun, F. Y. Su, X. X. Wei, X. M. Li, A. Ahmad, L. J. Xie and C. M. Chen, *J. Mater. Chem. A*, 2019, **7**, 16028–16045.
29 Y. Zheng, K. Chen, K. Jiang, F. Zhang, G. Zhu and H. Xu, *J. Energy Storage*, 2022, **56**, 105995.
30 M. Darder, P. Aranda and E. Ruiz-Hitzky, *Adv. Mater.*, 2007, **19**, 1309–1319.
31 W. S. Chen, H. P. Yu, S. Y. Lee, T. Wei, J. Li and Z. J. Fan, *Chem. Soc. Rev.*, 2018, **47**, 2837–2872.
32 S. H. Yang, Y. W. Cui, G. X. Yang, S. F. Zhao, J. Q. Wang, D. G. Zhao, C. Yang, X. T. Wang and B. Q. Cao, *J. Power Sources*, 2023, **554**, 232347.
33 X. Zhang, H. Li, B. Qin, Q. Wang, X. Xing, D. Yang, L. e. Jin and Q. Cao, *J. Mater. Chem. A*, 2019, **7**, 3298–3306.
34 A. K. Rana, E. Frollini and V. K. Thakur, *Int. J. Biol. Macromol.*, 2021, **182**, 1554–1581.
35 C. F. Ding, T. Y. Liu, X. D. Yan, L. B. Huang, S. O. Ryu, J. L. Lan, Y. H. Yu, W. H. Zhong and X. P. Yang, *Nano-Micro Lett.*, 2020, **12**, 63.
36 L. M. Chen, H. Y. Yu, Z. H. Li, X. Chen and W. L. Zhou, *Nanoscale*, 2021, **13**, 17837–17845.
37 M. Yu, J. Li and L. J. Wang, *Chem. Eng. J.*, 2017, **310**, 300–306.
38 B. Duan, Y. Huang, A. Lu and L. N. Zhang, *Prog. Polym. Sci.*, 2018, **82**, 1–33.
39 M. A. Meyers, J. McKittrick and P. Y. Chen, *Science*, 2013, **339**, 773–779.
40 L. Gao, G. Zhang, J. Cai, L. Huang, J. Zhou and L. Zhang, *Nano Res.*, 2020, **13**, 1604–1613.
41 M. Rinaudo, *Prog. Polym. Sci.*, 2006, **31**, 603–632.
42 M. Nasrollahzadeh, M. Sajjadi, S. Iravani and R. S. Varma, *Carbohydr. Polym.*, 2021, **251**, 116986.
43 J. Y. Huang, Y. R. Liang, H. Hu, S. M. Liu, Y. J. Cai, H. W. Dong, M. T. Zheng, Y. Xiao and Y. L. Liu, *J. Mater. Chem. A*, 2017, **5**, 24775–24781.
44 Y. Xi, Z. Xiao, H. Lv, H. Sun, S. Zhai and Q. An, *J. Colloid Interface Sci.*, 2023, **630**, 525–534.
45 T. Lyu, S. Lin, L. Mo, F. Wang and Z. Shao, *Int. J. Energy Res.*, 2022, **46**, 17056–17067.
46 Y. Sun, D. Xu and S. Wang, *Carbon*, 2022, **199**, 258–267.
47 M. Y. Yuan, Y. Q. Zhang, B. Niu, F. Jiang, X. N. Yang and M. Li, *J. Mater. Sci.*, 2019, **54**, 14456–14468.
48 M. Yuan, Y. Zhang, B. Niu, F. Jiang, X. Yang and M. Li, *J. Mater. Sci.*, 2019, **54**, 14456–14468.
49 Y. Tong, J. Y. Yang, J. J. Li, Z. Y. Cong, L. Wei, M. M. Liu, S. R. Zhai, K. Wang and Q. D. An, *J. Mater. Chem. A*, 2023, **11**, 1061–1082.
50 Q. N. Sun, R. Khunsupat, K. Akato, J. M. Tao, N. Labbe, N. C. Gallego, J. J. Bozell, T. G. Rials, G. A. Tuskan, T. J. Tschaplinski, A. K. Naskar, Y. Q. Pu and A. J. Ragauskas, *Green Chem.*, 2016, **18**, 5015–5024.
51 C. Jiang, Z. H. Wang, J. X. Li, Z. J. Sun, Y. F. Zhang, L. Li, K. S. Moon and C. P. Wong, *Electrochim. Acta*, 2020, 353.
52 N. N. Guo, M. Li, X. K. Sun, F. Wang and R. Yang, *Green Chem.*, 2017, **19**, 2595–2602.
53 H. Wang, F. Xiong, F. Guo, Y. Han, F. Chen, B. Ma, J. Yang, M. Wen, Y. Qing, F. Chu and Y. Wu, *Colloids Surf., A*, 2022, **655**, 130237.
54 Y. Y. Long, X. Y. An, H. Zhang, J. Yang, L. Q. Liu, Z. J. Tian, G. H. Yang, Z. B. Cheng, H. B. Cao, H. B. Liu and Y. H. Ni, *Chem. Eng. J.*, 2023, **451**, 138877.
55 X. Han, Q. Wei, Y. Su, G. Che, J. Zhou and Y. Li, *ACS Appl. Mater. Interfaces*, 2023, **15**, 1969–1983.
56 F. Torres-Canas, A. Bentaleb, M. Follmer, J. Roman, W. Neri, I. Ly, A. Derre and P. Poulin, *Carbon*, 2020, **163**, 120–127.
57 C. Jiang, Z. H. Wang, J. X. Li, Z. J. Sun, Y. F. Zhang, L. Li, K. S. Moon and C. P. Wong, *Electrochim. Acta*, 2020, **353**, 136482.
58 M. Hassan, M. A. Gondal, E. Cevik and A. Bozkurt, *ACS Appl. Energy Mater.*, 2022, **5**, 6833–6846.
59 H. W. Guo, A. T. Zhang, H. C. Fu, H. W. Zong, F. H. Jin, K. Zhao and J. Q. Liu, *Chem. Eng. J.*, 2023, **453**, 139633.
60 D. Li, C. Lv, L. Liu, Y. Xia, X. She, S. Guo and D. Yang, *ACS Cent. Sci.*, 2015, **1**, 261–269.
61 S. Sun, B. Ding, R. Liu and X. Wu, *J. Alloys Compd.*, 2019, **803**, 401–406.

62 Y. P. Lu, L. T. Liu, R. Zhang, Z. J. Jiang, Y. M. Li, Z. Y. Sun, X. H. Chen and H. H. Song, *Appl. Surf. Sci.*, 2022, **604**, 154631.
63 M. Nasrollahzadeh, M. Sajjadi, S. Iravani and R. S. Varma, *Carbohydr. Polym.*, 2021, 251.
64 G. Yuan, K. X. Guan, H. Hu, B. F. Lei, Y. Xiao, H. W. Dong, Y. R. Liang, Y. L. Liu and M. T. Zheng, *J. Colloid Interface Sci.*, 2021, **582**, 159–166.
65 C. H. Zhao, Y. X. Wang, J. X. Zheng, S. J. Xu, P. F. Rui and C. Zhao, *J. Power Sources*, 2022, **521**, 230942.
66 X. D. Luo, Y. Wang, Z. F. Shen, L. F. Cui, Y. G. Wang and X. Li, *J. Colloid Interface Sci.*, 2021, **599**, 351–359.
67 J. H. Jeong, Y. A. Kim and B. H. Kim, *Carbon*, 2020, **164**, 296–304.
68 J. Chen, Y. Huo, S. Li, Y. Huang and S. Lv, *Compos. Commun.*, 2019, **16**, 117–123.
69 H. Lin, Z. Tan, J. Yang, R. Mo, Y. Liang, M. Zheng, H. Hu, H. Dong, X. Liu, Y. Liu and Y. Xiao, *J. Energy Storage*, 2022, **53**, 105036.
70 X. T. Fu and S. M. Kim, *Mar. Drugs*, 2010, **8**, 200–218.
71 F. Zhang, T. Y. Liu, J. H. Zhang, E. T. Cui, L. Yue, R. Y. Jiang and G. H. Hou, *Carbon*, 2019, **147**, 451–459.
72 H. Liu, S. Zhu, Y. Zhang, H. Song, Y. Zhang, Y. Chang, W. Hou and G. Han, *Small*, 2023, 2204119.
73 J. Niu, R. Shao, M. Liu, Y. Zan, M. Dou, J. Liu, Z. Zhang, Y. Huang and F. Wang, *Adv. Funct. Mater.*, 2019, **29**, 201905095.
74 K. Gelse, E. Poschl and T. Aigner, *Adv. Drug Delivery Rev.*, 2003, **55**, 1531–1546.
75 H. Liu, W. Chen, H. Peng, X. Huang, S. Li, L. Jiang, M. Zheng, M. Xu and J. Zhu, *Electrochim. Acta*, 2022, **434**, 141312.
76 K. Subhani, X. Jin, N. Hameed, A. K. Lau, J. A. M. Ramshaw, V. Glattauer and N. V. Salim, *Mater. Today Sustain.*, 2022, 100152.
77 N. Yang, R. Shao, Z. P. Zhang, M. L. Dou, J. Niu and F. Wang, *Carbon*, 2021, **178**, 775–782.
78 G. J. Wang, Z. H. Lin, S. H. Jin, M. Li and L. Y. Jing, *J. Energy Storage*, 2022, **45**, 103525.
79 Q. Z. Du, Y. H. Zhao, K. L. Zhuo, Y. J. Chen, L. F. Yang, C. F. Wang and J. J. Wang, *Nanoscale*, 2021, **13**, 13285–13293.
80 X. M. Fan, C. Yu, J. Yang, Z. Ling, C. Hu, M. D. Zhang and J. S. Qiu, *Adv. Energy Mater.*, 2015, **5**, 201401761.
81 M. D. Zhang, C. Yu, Z. Ling, J. H. Yu, S. F. Li, C. T. Zhao, H. L. Huang and J. S. Qiu, *Green Chem.*, 2019, **21**, 2095–2103.
82 S. Y. Cho, H. J. Yoon, N. R. Kim, Y. S. Yun and H. J. Jin, *J. Power Sources*, 2016, **329**, 536–545.
83 Y. Sun, S. Xue, J. H. Sun, X. X. Li, Y. C. Ou, B. H. Zhu and M. Demir, *J. Colloid Interface Sci.*, 2023, **645**, 297–305.
84 K. Z. Gao, S. Y. Zhao, Q. Y. Niu and L. Z. Wang, *Cellulose*, 2019, **26**, 9241–9254.
85 M. A. Meyers, P. Y. Chen, A. Y. M. Lin and Y. Seki, *Prog. Mater. Sci.*, 2008, **53**, 1–206.
86 S. Wu, H. Zhou, Y. Zhou, H. Wang, Y. Li, X. Liu and Y. Zhou, *J. Alloys Compd.*, 2021, **859**, 157814.
87 S. M. Wu, H. Zhou, Y. H. Zhou, H. Wang, Y. H. Li, X. Q. Liu and Y. M. Zhou, *J. Alloys Compd.*, 2021, **859**, 157814.
88 P. Sinha, A. Yadav, A. Tyagi, P. Paik, H. Yokoi, A. K. Naskar, T. Kuila and K. K. Kar, *Carbon*, 2020, **168**, 419–438.
89 Y. N. Zhang, C. Y. Su, J. L. Chen, W. H. Huang and R. Lou, *Rare Met.*, 2022, **42**, 769–796.
90 L. Borchardt, M. Oschatz and S. Kaskel, *Mater. Horiz.*, 2014, **1**, 157–168.
91 B. Yan, J. Zheng, L. Feng, Q. Zhang, C. Zhang, Y. Ding, J. Han, S. Jiang and S. He, *Mater. Des.*, 2023, **229**, 111904.
92 S. Rawat, C. T. Wang, C. H. Lay, S. Hotha and T. Bhaskar, *J. Energy Storage*, 2023, **63**, 107115.
93 X. P. Li, J. U. Zhang, B. Liu, Z. P. Su and J. J. Klemes, *J. Cleaner Prod.*, 2021, **310**, 127428.
94 C. Young, T. Park, J. W. Yi, J. Kim, M. S. A. Hossain, Y. V. Kaneti and Y. Yamauchi, *ChemSusChem*, 2018, **11**, 3546–3558.
95 Y. F. Yin, Q. J. Liu, J. Wang and Y. T. Zhao, *Int. J. Hydrogen Energy*, 2022, **47**, 39338–39363.
96 Y. Li, Y. Sun, H. Li, M. Sun, J. Shen and S. Wang, *Energy*, 2023, **270**, 126942.
97 S. A. Bhat, V. Kumar, S. Kumar, A. E. Atabani, I. Anjum Badruddin and K. J. Chae, *Fuel*, 2023, **337**, 127125.
98 J. Yin, W. L. Zhang, N. A. Alhebshi, N. Salah and H. N. Alshareef, *Small Methods*, 2020, **4**, 1900853.
99 D. Meng, Y. Hu, Y. Jing, X. Zhang, S. Mahmud, S. Su and J. Zhu, *Fuel*, 2022, **320**, 124002.
100 Y. Gao, Q. Yue, B. Gao and A. Li, *Sci. Total Environ.*, 2020, **746**, 141094.
101 G. S. Jiang, R. A. Senthil, Y. Z. Sun, T. R. Kumar and J. Q. Pan, *J. Power Sources*, 2022, **520**, 230886.
102 Q. Cao, M. Zhu, J. Chen, Y. Song, Y. Li and J. Zhou, *ACS Appl. Mater. Interfaces*, 2020, **12**, 1210–1221.
103 Z. L. Yu, G. C. Li, N. Fechler, N. Yang, Z. Y. Ma, X. Wang, M. Antonietti and S. H. Yu, *Angew. Chem. Int. Ed.*, 2016, **55**, 14623–14627.
104 L. Y. Yang, J. Q. Li, Y. C. Zhou and J. F. Yao, *J. Energy Storage*, 2022, **50**, 104252.
105 Z. Zhai, B. Ren, Y. Xu, S. Wang, L. Zhang and Z. Liu, *J. Power Sources*, 2021, **481**, 228976.
106 X. Tong, Z. Chen, H. Zhuo, Y. Hu, S. Jing, J. Liu and L. Zhong, *Carbohydr. Polym.*, 2019, **207**, 764–774.
107 J. Yin, W. Zhang, N. A. Alhebshi, N. Salah and H. N. Alshareef, *Small Methods*, 2020, **4**, 1900853.
108 N. Díez, G. A. Ferrero, M. Sevilla and A. B. Fuertes, *J. Mater. Chem. A*, 2019, **7**, 14280–14290.
109 S. Wang, J. F. Feng and H. Pan, *Colloids Surf., A*, 2022, **651**, 129622.
110 J. Deng, T. Y. Xiong, F. Xu, M. M. Li, C. L. Han, Y. T. Gong, H. Y. Wang and Y. Wang, *Green Chem.*, 2015, **17**, 4053–4060.
111 Y. H. Wang, R. N. Liu, Y. D. Tian, Z. Sun, Z. H. Huang, X. L. Wu and B. Li, *Chem. Eng. J.*, 2020, **384**, 123263.
112 K. J. Zhang, M. R. Liu, T. Z. Zhang, X. Y. Min, Z. R. Wang, L. Y. Chai and Y. Shi, *J. Mater. Chem. A*, 2019, **7**, 26838–26848.
113 P. Wang, H. Ye, Y. X. Yin, H. Chen, Y. B. Bian, Z. R. Wang, F. F. Cao and Y. G. Guo, *Adv. Mater.*, 2019, **31**, 1805134.

114 F. Wang, J. Y. Cheong, J. Lee, J. Ahn, G. G. Duan, H. L. Chen, Q. Zhang, I. D. Kim and S. H. Jiang, *Adv. Funct. Mater.*, 2021, **31**, 2101077.
115 C. D. Liang, Z. J. Li and S. Dai, *Angew. Chem. Int. Ed.*, 2008, **47**, 3696–3717.
116 Q. Wang, W. Ma, E. Yin, S. Yu, S. Wang, H. Xiang, D. Li and M. Zhu, *ACS Appl. Energy Mater.*, 2020, **3**, 9360–9368.
117 Y. D. Zhong, T. Wang, M. Yan, C. Miao, X. F. Zhou and G. L. Tong, *Int. J. Biol. Macromol.*, 2022, **217**, 66–76.
118 C. Ma, L. Q. Wu, M. Dirican, H. Cheng, J. J. Li, Y. Song, J. L. Shi and X. W. Zhang, *J. Colloid Interface Sci.*, 2021, **586**, 412–422.
119 J. Cao, C. Zhu, Y. Aoki and H. Habazaki, *ACS Sustain. Chem. Eng.*, 2018, **6**, 7292–7303.
120 E. K. Kim, H. S. Chang, B. M. Lee, J. J. Park, J. M. Yun and J. H. Choi, *Sustainable Mater. Technol.*, 2022, **34**, e00520.
121 X. W. Liu, X. H. Liu, B. F. Sun, H. L. Zhou, A. P. Fu, Y. Q. Wang, Y. G. Guo, P. Z. Guo and H. L. Li, *Carbon*, 2018, **130**, 680–691.
122 G. J. Liang, L. G. Zhu, J. Xu, D. Fang, Z. K. Bai and W. L. Xu, *Electrochim. Acta*, 2013, **103**, 9–14.
123 Y. T. Qiu, M. Z. Hou, J. C. Gao, H. L. Zhai, H. M. Liu, M. M. Jin, X. Liu and L. F. Lai, *Small*, 2019, **15**, 1903836.
124 J. Lin, L. Yao, Z. Li, P. Zhang, W. Zhong, Q. Yuan and L. Deng, *Nanoscale*, 2019, **11**, 3281–3291.
125 H. Li, Y. H. Zhao, S. Q. Liu, P. C. Li, D. Yuan and C. B. He, *Microporous Mesoporous Mater.*, 2020, **297**, 109960.
126 L. Yao, J. Lin, Y. Chen, X. Li, D. Wang, H. Yang, L. Deng and Z. Zheng, *InfoMat*, 2022, **4**, e12278.
127 Q. Wu, M. M. Gao, S. S. Cao, J. Q. Hu, L. Huang, S. T. Yu and A. J. Ragauskas, *J. Taiwan Inst. Chem. Eng.*, 2019, **101**, 231–243.
128 X. Hou, H. Dang, M. Liu, X. Shang, Y. Fu and D. He, *J. Alloys Compd.*, 2019, **810**, 151736.
129 X. S. Zhang, W. B. Jian, L. Zhao, F. W. Wen, J. L. Chen, J. Yin, Y. L. Qin, K. Lu, W. L. Zhang and X. Q. Qiu, *Colloids Surf., A*, 2022, **636**, 128191.
130 L. Zhao, W. B. Jian, X. S. Zhang, F. W. Wen, J. H. Zhu, S. Huang, J. Yin, K. Lu, M. S. Zhou, W. L. Zhang and X. Q. Qiu, *J. Energy Storage*, 2022, **53**, 105095.
131 J. Pang, W. F. Zhang, J. L. Zhang, G. P. Cao, M. F. Han and Y. S. Yang, *Green Chem.*, 2017, **19**, 3916–3926.
132 J. W. Li, X. F. Li, D. B. Xiong, L. Z. Wang and D. J. Li, *Appl. Surf. Sci.*, 2019, **475**, 285–293.
133 Y. K. Fan, F. B. Fu, D. J. Yang, W. F. Liu, Z. X. Li and X. Q. Qiu, *J. Energy Storage*, 2023, **63**, 106947.
134 Y. F. Zheng, K. M. Chen, K. P. Jiang, F. R. Zhang, G. S. Zhu and H. R. Xu, *J. Energy Storage*, 2022, **56**, 105995.
135 Z. Bian, H. Wang, X. Zhao, Z. Ni, G. Zhao, C. Chen, G. Hu and S. Komarneni, *J. Colloid Interface Sci.*, 2023, **630**, 115–126.
136 F. B. Fu, D. J. Yang, B. W. Zhao, Y. K. Fan, W. F. Liu, H. M. Lou and X. Q. Qiu, *J. Colloid Interface Sci.*, 2023, **640**, 698–709.
137 X. Feng, Y. Bai, M. Q. Liu, Y. Li, H. Y. Yang, X. R. Wang and C. Wu, *Energy Environ. Sci.*, 2021, **14**, 2036–2089.
138 M. Seredych, D. Hulicova-Jurcakova, G. Q. Lu and T. J. Bandosz, *Carbon*, 2008, **46**, 1475–1488.
139 S. A. Wang, L. N. Dong, Z. Y. Li, N. Lin, H. Xu and S. M. Gao, *Int. J. Biol. Macromol.*, 2020, **164**, 4095–4103.
140 J. Q. Sun, J. Zhang, M. G. Shang, M. N. Zhang, X. F. Zhao, S. J. Liu, X. C. Liu, S. Liu and X. B. Yi, *Appl. Surf. Sci.*, 2023, **608**, 155109.
141 Y. Zhou, S. L. Candelaria, Q. Liu, Y. X. Huang, E. Uchaker and G. Z. Cao, *J. Mater. Chem. A*, 2014, **2**, 8472–8482.
142 X. Wang, M. Hou, Z. Shi, X. Liu, I. Mizota, H. Lou, B. Wang and X. Hou, *ACS Appl. Mater. Interfaces*, 2021, **13**, 12059–12068.
143 C. G. Hu and L. M. Dai, *Adv. Mater.*, 2019, **31**, 1804672.
144 Q. Abbas, R. Raza, I. Shabbir and A. G. Olabi, *J. Sci.: Adv. Mater. Devices*, 2019, **4**, 341–352.
145 J. Huang, W. Zhang, H. B. Huang, Y. L. Liu, Q. Y. Yang and L. Li, *ACS Sustain. Chem. Eng.*, 2019, **7**, 16710–16719.
146 B. B. Fan, S. M. Wu, H. Wang and Y. M. Zhou, *J. Electrochem. Soc.*, 2021, **168**, 100534.
147 S. Qiu, Z. Chen, H. Zhuo, Y. Hu, Q. Liu, X. Peng and L. Zhong, *ACS Sustain. Chem. Eng.*, 2019, **7**, 15983–15994.
148 Y. M. Wang, X. Wang, X. L. Li, Y. Bai, H. H. Xiao, Y. Liu, R. Liu and G. H. Yuan, *Adv. Funct. Mater.*, 2019, **29**, 1900326.
149 L. Ma, J. Liu, S. Lv, Q. Zhou, X. Shen, S. Mo and H. Tong, *J. Mater. Chem. A*, 2019, **7**, 7591–7603.
150 P. Zhang, J. P. Li, D. Y. Yang, R. A. Soomro and B. Xu, *Adv. Funct. Mater.*, 2022, **33**, 2209918.
151 R. Liu, A. Zhou, X. Zhang, J. Mu, H. Che, Y. Wang, T.-T. Wang, Z. Zhang and Z. Kou, *Chem. Eng. J.*, 2021, **412**, 128611.
152 K. Ren, Z. Liu, T. Wei and Z. J. Fan, *Nano-Micro Lett.*, 2021, **13**, 129.
153 S. Kumar, G. Saeed, L. Zhu, K. N. Hui, N. H. Kim and J. H. Lee, *Chem. Eng. J.*, 2021, **403**, 126352.
154 K. Zhao, X. Sun, Z. Wang, C. Huang, D. Li and J. Liu, *J. Alloys Compd.*, 2022, **921**, 166036.
155 X. Ning, F. Li, Y. Zhou, Y.-E. Miao, C. Wei and T. Liu, *Chem. Eng. J.*, 2017, **328**, 599–608.
156 H. Peng, J. Zhou, Z. Chen, R. Zhao, J. Liang, F. Wang, G. Ma and Z. Lei, *J. Alloys Compd.*, 2019, **797**, 1095–1105.
157 D. Wu and W. B. Zhong, *J. Mater. Chem. A*, 2019, **7**, 5819–5830.
158 N. Kumar, S. B. Kim, S. Y. Lee and S. J. Park, *Nanomaterials*, 2022, **12**, 3708.
159 H. Zhuo, Y. J. Hu, Z. H. Chen and L. X. Zhong, *Carbohydr. Polym.*, 2019, **215**, 322–329.
160 S. Liu, K. Wan, C. Zhang and T. Liu, *Compos. Commun.*, 2021, **24**, 100610.
161 F. B. Fu, H. Wang, D. J. Yang, X. Q. Qiu, Z. X. Li and Y. L. Qin, *J. Colloid Interface Sci.*, 2022, **617**, 694–703.
162 S. M. Mousavi, S. A. Hashemi, M. Y. Kalashgrani, A. Gholami, Y. Mazaheri, M. Riazi, D. Kurniawan, M. Arjmand, O. Madkhali, M. D. Aljabri, M. M. Rahman and W. H. Chiang, *Chem. Rec.*, 2023, 202200266.
163 J. L. Espinoza-Acosta, P. I. Torres-Chávez, J. L. Olmedo-Martínez, A. Vega-Rios, S. Flores-Gallardo and E. A. Zaragoza-Contreras, *J. Energy Chem.*, 2018, **27**, 1422–1438.
164 M. S. Rostami and M. M. Khodaei, *J. Energy Storage*, 2023, **72**, 108344.